Reviewed Preprint
v1 • March 13, 2025
Not revised

Reviewed Preprint
v2 • February 18, 2026
Revised by authors

For correspondence:
tsuda@phar.kyushu-u.ac.jp

* These authors contributed equally.

Competing interests: No competing interests declared

Funding: See page 20

Reviewing editor: John Streicher, The University of Arizona, United States

Descending locus coeruleus noradrenergic signaling to spinal astrocyte subset is required for stress-induced mechanical pain hypersensitivity

Riku Kawanabe-Kobayashi[1,*], Sawako Uchiyama[1,*], Kohei Yoshihara[1,*], Keisuke Koga[2], Daiki Kojima[1], Thomas McHugh[3], Izuho Hatada[4,5], Ko Matsui[6], Kenji F Tanaka[7], Makoto Tsuda[1,8]

[1]Department of Molecular and System Pharmacology, Graduate School of Pharmaceutical Sciences, Kyushu University, Fukuoka, Japan • [2]Department of Neurophysiology, Hyogo Medical University, Nishinomiya, Japan • [3]Laboratory for Circuit and Behavioral Physiology, RIKEN Center for Brain Science, Wako, Japan • [4]Laboratory of Genome Science, Biosignal Genome Resource Center, Institute for Molecular and Cellular Regulation, Gunma University, Maebashi, Japan • [5]Viral Vector Core, Gunma University Initiative for Advanced Research (GIAR), Maebashi, Japan • [6]Super-network Brain Physiology, Graduate School of Life Sciences, Tohoku University, Sendai, Japan • [7]Division of Brain Sciences, Institute for Advanced Medical Research, Keio University School of Medicine, Tokyo, Japan • [8]Kyushu University Institute for Advanced Study, Fukuoka, Japan

eLife Assessment

This **important** study identifies a novel role for Hes5+ astrocytes in modulating the activity of descending pain-inhibitory noradrenergic neurons from the locus coeruleus during stress-induced pain facilitation. The role of glia in modulating neurological circuits including pain is poorly understood, and in that light, the role of Hes5+ astrocytes in this circuit is a key finding with broader potential impacts. This work is supported by **convincing** evidence, albeit somewhat limited by the indirect nature of the evidence linking adenosine to nearby neuronal modulation, and possible questions on the population specificity of the transgenic approach.

https://doi.org/10.7554/eLife.104453.2.sa4

Abstract

It is known that stress powerfully alters pain, but its underlying mechanisms remain elusive. Here, we identified a circuit, locus coeruleus descending noradrenergic neurons projecting to the spinal dorsal horn ($LC^{\rightarrow SDH}$-NA neurons), that is activated by acute exposure to restraint stress and is required for stress-induced mechanical pain hypersensitivity in mice. Interestingly, the primary target of spinal NA released from descending $LC^{\rightarrow SDH}$-NAergic terminals causing the stress-induced pain hypersensitivity was α_{1A}-adrenaline receptors (α_{1A}Rs) in Hes5-positive ($Hes5^{+}$) astrocytes located in the SDH, an astrocyte subset that has an ability to induce pain sensitization. Furthermore, activation of $Hes5^{+}$ astrocytes reduced activity of SDH-inhibitory neurons (SDH-INs) that have an inhibitory role in pain processing. This astrocytic reduction of IN activity was canceled by an A_1-adenosine receptor (A_1R)-knockdown in SDH-INs, and the A_1R-knockdown suppressed pain hypersensitivity caused by acute restraint stress. Therefore, our findings suggest that $LC^{\rightarrow SDH}$-NA neuronal signaling to $Hes5^{+}$ SDH astrocytes and subsequent astrocytic reduction of SDH-IN activity are essential for mechanical pain facilitation caused by stress.

Introduction

Somatosensory information generated at the periphery, such as skin, is conveyed to the dorsal horn of the spinal cord (SDH) via primary afferent sensory neurons and further to the brain[1,2]. The SDH is the first region for processing the peripherally derived sensory information and thus is critical for its proper transmission to and perception in the brain[1–6]. The processing of somatosensory information is not only tightly regulated by complex neuronal circuits within the SDH but also powerfully modulated by descending neurons from the brain[7,8]. The locus coeruleus (LC), a small nucleus located in the brainstem, modulates pain information processing in the SDH via descending noradrenaline (NA) neurons[8–11]. Activation of SDH-projecting LC-NA ($LC^{\rightarrow SDH}$-NA) neurons leads to a release of NA in the SDH[12]. Spinal NA acts on α_{1A}-adrenaline receptors (α_{1A}Rs) expressed on inhibitory neurons (INs)[13,14] and facilitates γ-aminobutyric acid (GABA)-mediated inhibitory synaptic transmission[15,16]. This NA signal has been implicated in the inhibitory control of nociceptive information processing[9–11]. Besides neurons, glial cells in the SDH, such as microglia and astrocytes, also have a remarkable ability to modulate the processing and transmission of somatosensory information[17–19]. Glial modulation has been extensively studied in pathological settings[17–19], but studies using *in vivo* imaging have shown that SDH astrocytes respond to noxious stimuli applied to the periphery under normal conditions[20–23]. Furthermore, we have recently identified a subset of spinal astrocytes defined by expression of hairy and enhancer of split 5 (Hes5) as a new target of NA[22]. Astrocytes express various types of adrenaline receptors[24]; activation of $LC^{\rightarrow SDH}$-NA neurons induces an increase in intracellular Ca^{2+} ($[Ca^{2+}]_i$), an indicator of astrocyte activity[25], via α_{1A}Rs[22], which are the most abundant adrenaline receptors in astrocytes[26,27]. $Hes5^+$ astrocytes are selectively distributed in the superficial laminae of SDH where it receives primary afferent sensory fibers. Activation of α_{1A}Rs of $Hes5^+$ SDH astrocytes by intrathecal administration of NA induces pain sensitization to light mechanical stimuli applied to the skin[22]. Given that most of the varicosities of NAergic axons/terminals are located closer to astrocytic processes than to neuronal synapses[28], $Hes5^+$ astrocytes could be a critical NA target for modulating pain in the SDH.

LC-NA neurons are known to respond to several external and internal stressors[29]. In rodent models of stress, nociceptive stimuli (e.g., electric shock, animal bite, etc.) are frequently employed as stressors. LC-NA neurons respond not only to stimuli that directly excite nociceptors[30,31], but also to stressors that do not involve their direct stimulation[30,32]. Several studies using rodent stress models have shown that exposure to stressors with or without nociceptor activation induces a remarkable change in pain-associated behavior[33,34]. Despite the impact of stress on the pain system, the mechanism underlying a link between stress and pain, especially pain exacerbation, at the neural circuit and cellular levels remains poorly understood, although it has been proposed that activation of enkephalinergic and GABAergic INs in the SDH is involved in stress-induced pain inhibition[35]. Since stressful events are known to have a significant impact on chronic pain[36,37], providing new insights into the mechanisms by which stress modulates pain is also of clinical importance.

In this study, we investigated how stress modulates pain with a focus on $LC^{\rightarrow SDH}$-NA neurons and their target $Hes5^+$ astrocytes in the SDH, using multiple approaches. Our experiments using *in vivo* Ca^{2+} imaging, chemogenetics and optogenetics, cell ablation, electrophysiology, biochemical imaging for NA release and astrocytic Ca^{2+} responses, conditional gene knockout, and behavioral analyses demonstrate for the first time that $LC^{\rightarrow SDH}$-NA neuronal signaling to $Hes5^+$ SDH astrocytes and subsequent astrocytic reduction of SDH-IN activity are essential for stress-induced mechanical pain hypersensitivity.

Results

LC$^{\rightarrow SDH}$-NA neurons mediate mechanical hypersensitivity after acute restraint stress

To investigate the mechanism underlying stress-induced pain modulation, we subjected wild-type (WT) mice to acute restraint stress exposure (Figure 1A), a well-known and frequently used stress model[29]. Consistent with a previous study[38], restraint stress for 30 min and 1 hour induced hypersensitivity to light mechanical stimuli (by applying von Frey filaments) to the plantar skin of the hindpaw (Figure 1B). However, with longer exposure (2 hours) to restraint stress, mechanical hypersensitivity was attenuated (Figure S1). In addition, mice subjected to 2-hour restraint stress displayed antinociceptive responses to noxious heat stimuli (the hot-plate test) (Figure S2), which is consistent with our previous finding[16] as well as numerous other reports (Table S1). In contrast to restraint stress, forced swim stress, which has been reported to produce antinociceptive effects on noxious heat[39], did not change mechanical pain sensitivity (Figure S2). Thus, our data suggest that under our experimental conditions, single exposure of 1-hour restraint stress causes behavioral pain hypersensitivity to mechanical stimuli, although stress-induced modulation of pain is a complex phenomenon influenced by multiple factors, including the stress model, intensity, and duration, as well as the sensory modality used for behavioral testing.

Since 1-hour exposure to restraint stress has also been reported to increase plasma corticosterone levels[40], in subsequent experiments, we chose 1 hour as the exposure time to restraint stress. To analyze LC-NA neuronal activity during restraint stress, we performed fiber photometry using *NET-Cre* mice (Cre is expressed in NAergic neurons under the control of the promoter of NA transporter [NET])[41] with microinjection into the LC of an adeno-associated viral (AAV) vector designed to express GCaMP6s (genetic encoded fluorescent Ca^{2+} indicator) in a Cre-dependent manner (AAV-FLEx[GCaMP6s]). Three weeks after the injection, GCaMP6s was expressed selectively in tyrosine hydroxylase^{+} (TH^{+}) LC-NA neurons (Figure 1C)[42]. We found that restraint stress exposure increased the number of Ca^{2+} events in these neurons (Figure 1, D and E; Figure S3; Movie). The number of Ca^{2+} events was highest during the first 20 min of the restraint stress exposure and gradually decreased later.

To investigate the role of LC-NA neurons in mechanical hypersensitivity, we utilized a cell ablation approach[43]; diphtheria toxin (DTX) receptors (DTR) were specifically expressed in LC-NA neurons by injection of AAV-FLEx[DTR-EGFP] into the LC of *NET-Cre* mice (Figure 1F). DTR^{+} neurons (detected by GFP) mainly co-expressed TH, and these neurons were ablated by DTX administration (10 μg/kg, two injections 24-hour apart), which resulted in a loss of TH signal in the LC and reduction of NET signal in the SDH (Figure 1G). We performed behavioral tests in these mice and observed that ablation of LC-NA neurons abolished mechanical hypersensitivity after restraint stress exposure (Figure 1H). To specifically ablate LC$^{\rightarrow SDH}$-NA neurons, a retrograde AAV vector expressing Cre (AAVretro-Cre) was injected into the L4 SDH, followed by AAV-FLEx[DTR-EGFP] injection into the LC (Figure 1I). In these mice, TH^{+} LC$^{\rightarrow SDH}$-NA neurons expressing DTR (detected by EGFP) were ablated after DTX administration (Figure 1J; Figure S4, A and B) (4.4% of total TH^{+} neurons in the LC (189 DTR^{+} cells per 4398 TH^{+} cells, n = 3 mice)). DTR^{+} cells were not observed in A5 or A7 (Figure S4C), confirming the specificity of LC$^{\rightarrow SDH}$-NAergic pathway targeting in our study. These mice also failed to induce

mechanical hypersensitivity after the restraint stress (Figure 1K). These results suggest that descending LC$^{\rightarrow SDH}$-NA neurons are necessary for mechanical pain hypersensitivity after acute restraint stress exposure. In contrast, motor behavior in the rotarod test and behavioral sensitivity to heat stimuli in the paw-flick test were not affected by ablation of LC$^{\rightarrow SDH}$-NA neurons (Figure

S5), indicating that ablation of these neurons does not produce non-specific behavioral deficits in motor function or other sensory modalities. Furthermore, we tested whether optogenetic activation of LC$^{\rightarrow SDH}$-NA neurons could induce mechanical hypersensitivity, using ChrimsonR, a well-established red-shifted channelrhodopsin[44]. *NET-Cre* mice were microinjected with AAV-

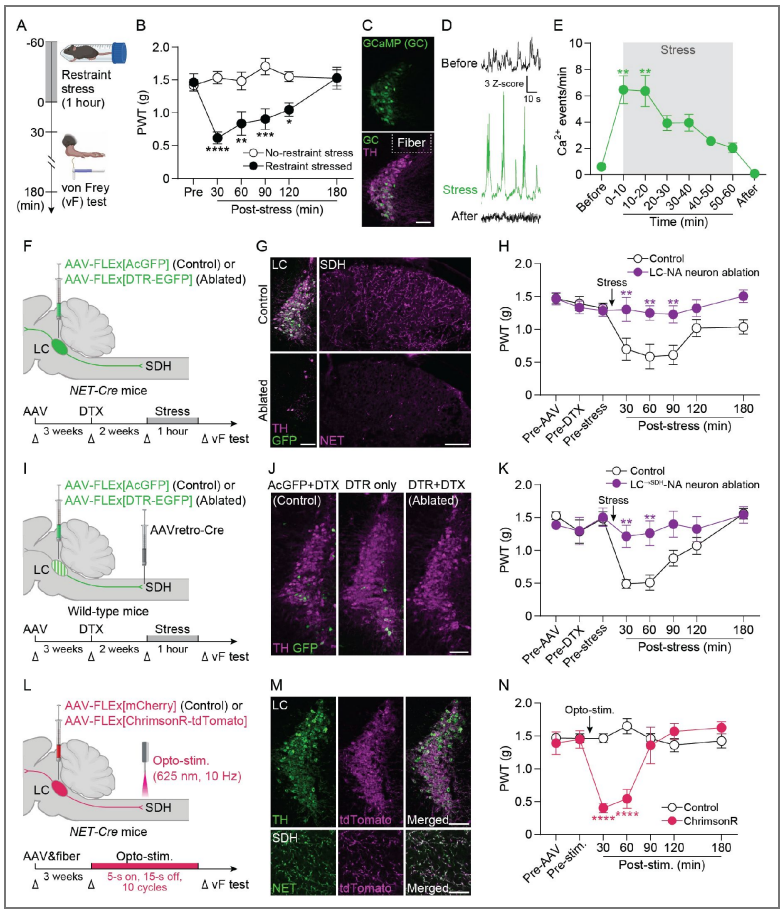

Figure 1. LC$^{\rightarrow SDH}$-NA neurons mediate stress-induced mechanical hypersensitivity.

(A) Schematic illustration of an experiment to investigate the effects of acute exposure to restraint stress (1 hour) on mechanosensory behavior in mice, using von Frey (vF) filaments. (B) Change in paw withdrawal threshold (PWT) measured by vF filaments in wild-type mice after restraint stress (n = 6 mice per group; two-way ANOVA with post hoc Bonferroni's multiple comparisons test; *P < 0.05, **P < 0.01, ***P < 0.001, ****P <0.0001 vs. no-restraint stress group). (C) Expression of GCaMP6s (GC; green) in the LC at 3 weeks after intra-LC injection of AAV-FLEx[GCaMP6s] in *NET-Cre* mice. TH immunofluorescence is shown in magenta. Dashed line indicates the location of the implanted optic fiber. Scale bar, 100 µm. (D and E) Representative traces and change in the frequency of GCaMP6s signals in LC-NA neurons (n = 6 mice; Friedman test with post hoc Dunn's multiple comparisons test; **P < 0.01 vs. the data of 'Before'). Traces shown at the top, middle, and bottom (D) indicate Ca^{2+} signals before, during, and after restraint stress, respectively. (F) Schematic illustration of the strategy of ablating LC-NA neurons using AAV vectors incorporating DTR (fused with EGFP) injected into the LC in *NET-Cre* mice. (G) TH immunofluorescence (magenta) and GFP (green) in the LC (left) and NET immunofluorescence (magenta) in the SDH (right) after administration of DTX (10 µg/kg, i.p., two injections 24 h-apart) in control mice (top) and DTR-expressing mice (bottom). Scale bars, 100 µm. (H) Effect of ablation of LC-NA neurons on PWT changes after acute restraint stress (n = 7 mice per group; two-way ANOVA with post hoc Bonferroni's multiple comparisons test; **P < 0.01 vs. control group). (I) Schematic illustration of the strategy of ablating LC$^{\rightarrow SDH}$-NA neurons using a retrograde AAV vector incorporating Cre injected into the SDH and an AAV vector incorporating DTR (fused with EGFP) injected into the LC in wild-type mice. (J) Representative images of LC$^{\rightarrow SDH}$-NA neurons in control or DTR-expressing mice treated with vehicle or DTX administration, respectively. GFP (green) and TH (magenta). Scale bar, 100 µm. (K) Effect of ablation of LC$^{\rightarrow SDH}$-NA neurons on PWT changes after restraint stress (n = 11 mice per group; two-way ANOVA with post hoc Bonferroni's multiple comparisons test; **P < 0.01 vs. control group). (L) Schematic illustration of the strategy for activating LC$^{\rightarrow SDH}$-NA neuronal axons/terminals using an AAV vector incorporating ChrimsonR (fused with tdTomato) injected into the LC in *NET-Cre* mice and of an optic cannula implanted in the SDH. (M) Representative images of TH (green) and tdTomato (magenta) expression in the LC (top) and NET (green) and tdTomato (magenta) expression in the SDH (bottom) at 3 weeks after intra-LC injection of AAV-FLEx[ChrimsonR-tdTomato] in *NET-Cre* mice. Scale bars, 100 µm (top) and 50 µm (bottom). (N) PWT before and after optogenetic stimulation (opto-stim.) in LC$^{\rightarrow SDH}$-NA axons/terminals (625 nm, 2 mW, 10 Hz, 5-ms pulse duration, 5-s light on, 15-s light off, 10 cycles) (Control, n = 4 mice; ChrimsonR, n = 5 mice; two-way ANOVA with post hoc Bonferroni's multiple comparisons test; ****P <0.0001 vs. control group). Data represent mean ± SEM. Created with *BioRender.com*. See also Figures S1–S6.

FLEx[ChrimsonR-tdTomato] into the LC (Figure 1L). Three weeks later, we confirmed expression of ChrimsonR (detected by tdTomato) in TH^+ neurons in the LC and NET^+ axons/terminals in the SDH (Figure 1M; Figure S6). Optogenetic stimulation of $LC^{\rightarrow SDH}$-NA neuronal axons/terminals in the SDH evoked mechanical hypersensitivity in these mice (Figure 1N). These results together demonstrate that $LC^{\rightarrow SDH}$-NA neurons are activated by acute stress exposure and are not only necessary for stress-induced mechanical pain hypersensitivity but also sufficient to phenocopy the behavioral response.

$LC^{\rightarrow SDH}$-NAergic signaling to $Hes5^+$ SDH astrocytes is required for stress-induced mechanical hypersensitivity

To investigate the mechanism by which activation of $LC^{\rightarrow SDH}$-NA neurons induces mechanical hypersensitivity, we first examined if NA is released in the SDH when these neurons are stimulated, using the genetically encoded fluorescent NA sensor $GRAB_{NE1m}$[45]. In spinal cord slices from *NET-Cre* mice that had been injected AAV-FLEx[ChrimsonR-tdTomato] into the LC and AAV-gfaABC$_1$D-$GRAB_{NE1m}$ (expressing $GRAB_{NE1m}$ under the control of the astrocyte-selective promoter gfaABC$_1$D[46] into the SDH) (Figure 2A), optogenetic stimulation of $LC^{\rightarrow SDH}$-NA axons/terminals increased $GRAB_{NE1m}$ fluorescence intensity (Figure 2B), confirming NA release from $LC^{\rightarrow SDH}$-NA neuron terminals in our slice conditions. The fluorescence intensity increased in a stimulation period-dependent manner (Figure 2C). Next, to determine the target cells and receptors of $LC^{\rightarrow SDH}$-NA neurons, we focused on α_{1A}Rs in astrocytes because our previous study showed that NA increases $[Ca^{2+}]_i$ in astrocytes via α_{1A}Rs[22]. Using spinal cord slices from *NET-Cre* mice that had been injected with AAV-FLEx[ChrimsonR-tdTomato] into the LC and AAV-gfaABC$_1$D-GCaMP6m into the SDH (Figure 2A), we found that optogenetic stimulation of $LC^{\rightarrow SDH}$-NA axons/terminals evoked a rise in $[Ca^{2+}]_i$ in astrocytes (Figure 2, D and E). Pretreatment with the α_{1A}R-specific antagonist silodosin (40 nM) suppressed the Ca^{2+} responses (Figure 2F), suggesting that NA released from $LC^{\rightarrow SDH}$-NA neurons induces Ca^{2+} responses in SDH astrocytes via α_{1A}Rs. Behaviorally, intrathecal injection of silodosin in *NET-Cre*;AAV-ChrimsonR mice attenuated mechanical hypersensitivity by optogenetic stimulation of the $LC^{\rightarrow SDH}$-NA neurons (Figure 2G). Consistent with our previous findings[22], intrathecal administration of NA (0.1 nmol) evoked transient mechanical hypersensitivity, which was completely abolished in *Hes5-CreERT2*;*Adra1a*$^{flox/flox}$ mice treated with tamoxifen ($Hes5^+$ astrocyte-selective conditional knockout of α_{1A}Rs[22]: $Hes5^+$ astrocyte–α_{1A}R cKO) (Figure 2H). Moreover, mechanical hypersensitivity after acute restraint stress was abolished in $Hes5^+$ astrocyte–α_{1A}R cKO mice (Figure 2I). In addition, intrathecal administration of 5,7-dichlorokynurenic acid (DCK; 10 nmol), an antagonist of D-serine signaling on N-methyl-D-aspartate (NMDA) receptors, also suppressed mechanical hypersensitivity (Figure 2J). Supporting this finding, our previous report identified D-serine as a hypersensitivity-inducing factor released from $Hes5^+$ astrocytes[22]. These results indicate that spinally-released NA from $LC^{\rightarrow SDH}$-NA neurons after acute restraint stress activates α_{1A}Rs on $Hes5^+$ astrocytes, which causes mechanical pain hypersensitivity.

$Hes5^+$ astrocytes mask IN function via adenosine A_1 receptors

Besides astrocytes, *Adra1a* mRNA is also expressed in INs in the SDH[13,14]. However, *Vgat-Cre*;*Adra1a*$^{flox/flox}$ mice ($Vgat^+$ IN-selective conditional knockout of α_{1A}Rs: $Vgat^+$ IN–α_{1A}R cKO mice)[14,16] had no effect on the NA (0.1 nmol)-induced mechanical hypersensitivity (Figure 3A). A similar behavioral phenotype was also observed after intrathecal administration of phenylephrine (0.05 nmol), a selective agonist for α_1Rs (Figure 3B). Furthermore, stress-induced mechanical hypersensitivity was not affected in $Vgat^+$ IN–α_{1A}R cKO mice (Figure 3C). Considering previous data that SDH-INs (including $Vgat^+$) respond to NA via α_{1A}Rs at NA concentrations similar to those that elicit $Hes5^+$ astrocyte response[16,22], it remains unclear why intrathecally administered NA and spinally released NA from $LC^{\rightarrow SDH}$-NA neuron terminals (after acute restraint stress) have no suppressive effect via α_{1A}R-mediated $Vgat^+$ IN activation on mechanical hypersensitivity. We then hypothesized an interaction between $Hes5^+$ astrocytes and $Vgat^+$ INs as per a previous report that

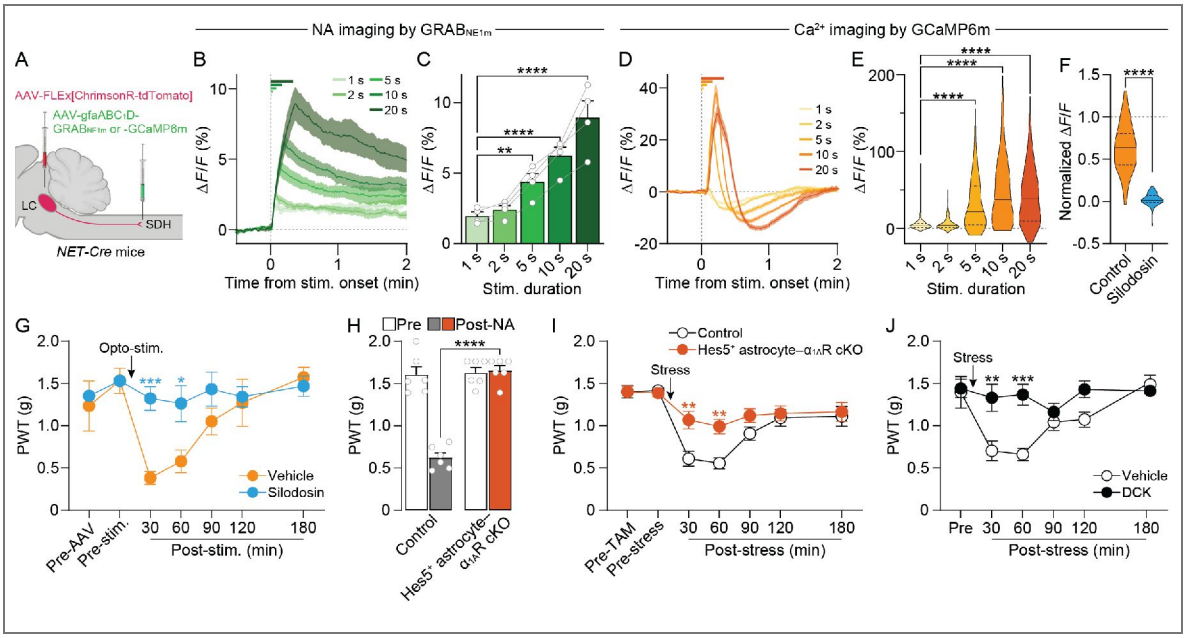

Figure 2. α_{1A}Rs in Hes5$^+$ SDH astrocytes are required for stress-induced mechanical hypersensitivity.

(A) Schematic illustration of intra-SDH microinjection of AAV-gfaABC$_1$D-GRAB$_{NE1m}$ or -GCaMP6m and intra-LC microinjection of AAV-FLEx[ChrimsonR-tdTomato] in *NET-Cre* mice. (B) Representative traces of GRAB$_{NE1m}$ signals by fluorescence imaging using spinal cord slices. Each trace represents the GRAB$_{NE1m}$ signal before and after optogenetic stimulation (625 nm, 1 mW, 10 Hz, 5 ms pulse duration, 1– 20 s). (C) Quantitative analysis of the peak amplitude of GRAB$_{NE1m}$ Δ*F*/*F* after optogenetic stimulation in LC$^{\rightarrow SDH}$-NA axons/terminals (n = 4 slices; one-way ANOVA with post hoc Dunnett's multiple comparisons test; **P < 0.01, ****P <0.0001). (D) Representative traces of astrocytic GCaMP6m signals by fluorescence imaging using spinal cord slices. Each trace represents the GCaMP6m signal before and after optogenetic stimulation (as described in B). (E) Quantitative analysis of the peak amplitude of GCaMP6m Δ*F*/*F* after optogenetic stimulation in LC$^{\rightarrow SDH}$-NA axons/terminals (n = 133 cells, 4 slices, 4 mice; Friedman test with post hoc Dunn's multiple comparisons test; ****P <0.0001). (F) Effect of silodosin (40 nM) on astrocytic Ca^{2+} responses in the SDH after optogenetic stimulation (10 s) in LC$^{\rightarrow SDH}$-NA axons/terminals (Control, n = 83 cells, 4 slices, 4 mice; Silodosin, n = 53 cells, 4 slices, 4 mice; Mann-Whitney test; ****P <0.0001). (G) Effect of intrathecal silodosin (3 nmol) on mechanical hypersensitivity induced by optogenetic stimulation in LC$^{\rightarrow SDH}$-NA axons/terminals (Vehicle, n = 5 mice; Silodosin, n = 6 mice; two-way ANOVA with post hoc Bonferroni's multiple comparisons test; *P < 0.05, ***P < 0.001 vs. vehicle group). (H) Change in PWT at 30 min after intrathecal injection of NA (0.1 nmol) in control (*Adra1a*$^{flox/flox}$) and Hes5$^+$ astrocyte-selective α$_{1A}$R conditional knockout mice [*Hes5-CreERT2*;*Adra1a*$^{flox/flox}$ mice treated with tamoxifen (TAM) (Hes5$^+$ astrocyte–α$_{1A}$R cKO mice) (n = 6 mice per group; two-way ANOVA with post hoc Bonferroni's multiple comparisons test; ****P <0.0001). (I and J) Stress-induced mechanical hypersensitivity in Hes5$^+$ astrocyte–α$_{1A}$R cKO mice [I: Control (*Adra1a*$^{flox/flox}$), n = 7 mice; Hes5$^+$ astrocyte–α$_{1A}$R cKO, n = 8 mice] or wild-type mice with intrathecal DCK (10 nmol) (J: n = 5 mice per group) (two-way ANOVA with post hoc Bonferroni's multiple comparisons test; **P < 0.01, ***P < 0.001 vs. control or vehicle group). Data represent mean ± SEM. Created with *BioRender.com*.

optogenetic activation of rat SDH astrocytes leads to ATP release; ATP is converted to adenosine extracellularly which subsequently suppresses the activity of SDH-INs via adenosine A_1 receptors (A_1Rs)[47]. By performing whole-cell current-clamp recordings of Vgat$^+$ INs in spinal cord slices from *Vgat-Cre*;*Rosa-tdTomato* mice, we found that bath application of NA (20 μM) evoked depolarization in 22.2% (10/45 cells) of tdTomato$^+$ cells (Vgat$^+$ INs), with 30% of these showing action potentials (3/10 cells) (Figure 3D). In our experiments, four antagonists for AMPA and NMDA receptors and $GABA_A$ and glycine receptors were added to the aCSF to block synaptic inputs from other neurons to the recorded Vgat$^+$ neurons[48,49], suggesting that NA directly acts on the recorded SDH Vgat$^+$ neurons to produce excitation. The proportion of Vgat$^+$ INs depolarized by NA is similar to that of *Adra1a* mRNA-expressing INs[14]. In 50% (5/10 cells) of depolarized Vgat$^+$ INs, additional application of the A_1R-selective agonist N6-cyclopentyladenosine (CPA; 1 μM) suppressed NA-induced depolarization/action potentials (Figure 3, D and E). Supporting this finding, RNAscope *in situ* hybridization detected *Adora1* mRNA fluorescence in 63.5 ± 6.9% of *Slc32a1* (*Vgat*)$^+$ INs (n = 497, from three mice) (Figure 3F). Because A_1Rs are also expressed in the dorsal root ganglion neurons[50], excitatory neurons and microglia[51] in the SDH, we employed the CRISPR–Cas9 system using AAV vectors to specifically knockdown A_1Rs in SDH-INs. AAV vectors designed to express the *Staphylococcus aureus* Cas9 (SaCas9)[52] in a Cre-dependent manner (AAV-FLEx[SaCas9]) and single guide RNA-expression vectors (AAV-FLEx[mCherry]-U6-sgAdora1 or -FLEx[mCherry]-U6-sgYFP [as a control]) were co-microinjected into the SDH of *Vgat-Cre* mice (Figure 3G). SaCas9 (detected by HA-tag) and mCherry-labeled cells in the SDH were immunolabeled with paired box 2 (PAX2) (Figure 3G), a marker of INs[53]. In these SDH-Vgat$^+$ IN-selective A_1R conditional knockdown mice (SDH-Vgat$^+$ IN–A_1R cKD mice), the inhibitory effect of CPA on NA-induced depolarization/action potentials was completely abolished in mCherry$^+$ neurons (Figure 3, H and I). Using a chemogenetic approach with modified human muscarinic G_q-protein-coupled receptors (hM3Dq)[54], we further examined the effect of G_q-stimulated Hes5$^+$ astrocytes on inhibitory synaptic transmission. *Hes5-CreERT2* mice were microinjected with AAV-FLEx[hM3Dq-HA] into the SDH (*Hes5-CreERT2*;AAV-hM3Dq mice). hM3Dq (detected by HA-tag) was expressed in the SDH, and these cells were double-labeled with glial fibrillary acidic protein (GFAP) and SRY-related high-mobility group box 9 (SOX9), markers of astrocytes (Figure 3J). Our previous studies using *Hes5-CreERT2* mice have confirmed that hM3Dq is not expressed in other cell types (neurons, oligodendrocytes, or microglia)[22,55]. Using spinal cord slices from these mice, we performed whole-cell voltage-clamp recordings of substantia gelatinosa (SG) neurons. Bath application of hM3Dq agonist clozapine N-oxide (CNO; 100 μM) reduced the frequency of spontaneous inhibitory postsynaptic currents (sIPSCs) in SG neurons (Figure 3, K and L). The concentration of CNO has been used in our previous study[22] but is relatively high; however, 100 μM CNO most effectively replicated the NA-induced Ca^{2+} signals in astrocytes (Figure S7, A and B). In addition, spinal cord slices from mice that did not express hM3Dq, 100 μM CNO had no effect on Ca^{2+} responses in SDH astrocytes (Figure S7A) and sIPSCs in SG neurons (Figure S7C), confirming that the observed effect of CNO is not non-specific. The reduction of sIPSCs by astrocytic hM3Dq activation was prevented by pretreatment with the A_1R-specific antagonist, 8-cyclopentyl-1,3-dimethylxanthine (CPT; 1 μM) (Figure 3, M and N). These results suggest that a signaling pathway from Hes5$^+$ astrocytes suppresses the activity of Vgat$^+$ INs via A_1Rs in the SDH.

Hes5$^+$ astrocyte-mediated inhibitory signals to INs affect mechanical hypersensitivity

We investigated whether A_1Rs in SDH-Vgat$^+$ INs contributed to the mechanical hypersensitivity elicited by intrathecal NA (0.1 nmol). Acute inhibition of spinal A_1Rs by intrathecal administration of CPT (3 nmol) suppressed NA-induced mechanical hypersensitivity (Figure 4A). Similarly, SDH-Vgat$^+$ IN–A_1R cKD mice showed a significant reduction in the behavioral hypersensitivity by NA (Figure 4B), indicating that A_1Rs in SDH-Vgat$^+$ INs contribute to mechanical hypersensitivity by spinal NA. Furthermore, SDH-Vgat$^+$ IN–A_1R cKD mice and intrathecal-CPT-pretreated mice exhibited a significant attenuation of the stress-induced mechanical hypersensitivity (Figure 4, C and D). These results suggest that Hes5$^+$ astrocyte-mediated negative control for SDH-Vgat$^+$

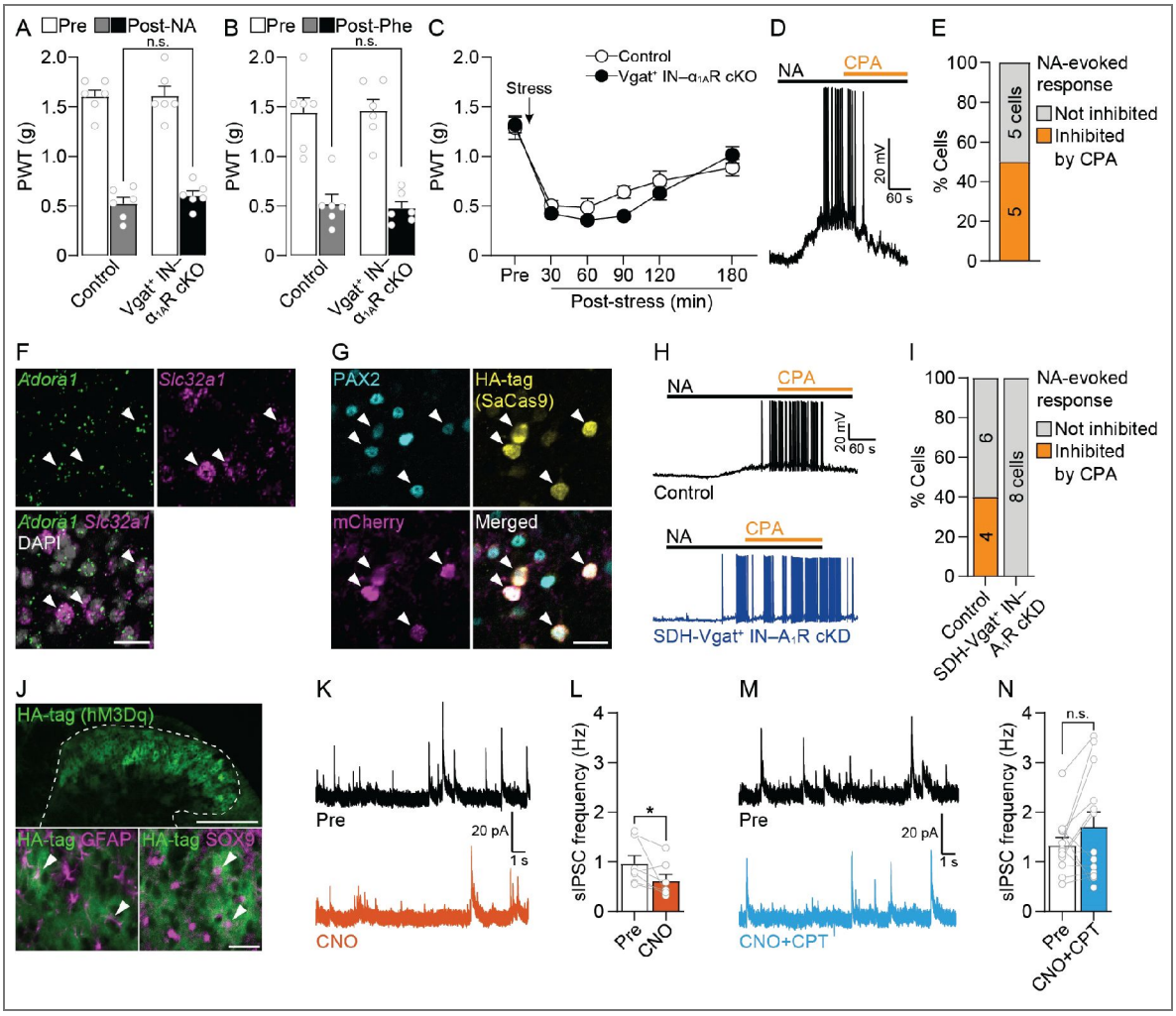

Figure 3. Activation of Hes5^{+} astrocytes reduces activity in Vgat^{+} INs in the SDH.

(A and B) Intrathecal NA (A, 0.1 nmol) or Phe (B, 0.05 nmol)-induced mechanical hypersensitivity in control (*Adra1a*$^{flox/flox}$) and Vgat^{+} IN-selective α_{1A}R conditional knockout mice [*Vgat-Cre*;*Adra1a*$^{flox/flox}$ mice (Vgat^{+} INs–α_{1A}R cKO mice)] (n = 6 mice per group; two-way ANOVA with post hoc Bonferroni's multiple comparisons test; n.s., not significant). (C) Changes in PWT after acute exposure to restraint stress in control (*Adra1a*$^{flox/flox}$; *n* = 6 mice) and Vgat^{+} INs–α_{1A}R cKO mice (*n* = 9 mice) (two-way ANOVA with post hoc Bonferroni's multiple comparisons test). (D) Representative trace of membrane potentials in tdTomato^{+} (Vgat^{+}) SDH neurons after application of NA (20 μM) to spinal cord slices from *Vgat-Cre*;*Rosa-tdTomato* mice. A_1R agonist CPA (1 μM) was co-applied with NA. (E) Percentage of Vgat^{+} SDH neurons whose NA-evoked response was inhibited by CPA (*n* = 10 cells from 7 mice). (F) Representative images of *Adora1* (A_1R) mRNA expression (green) in *Slc32a1* (Vgat)$^{+}$ INs (magenta). DAPI staining is shown in gray. Arrowheads indicate A_1R-expressing Vgat^{+} cells. Scale bar, 25 μm. (G) SaCas9 (yellow, detected by HA-tag) and mCherry (magenta) expression in the PAX2^{+} INs (cyan) at 3 weeks after intra-SDH injection of AAV-FLEx[SaCas9] and AAV-FLEx[mCherry]-U6-sgAdora1 in *Vgat-Cre* mice. Arrowheads indicate genome-editing Vgat^{+} cells. Scale bar, 25 μm. (H) Representative traces of membrane potentials in Vgat^{+} INs after application of NA and CPA to spinal cord slices from *Vgat-Cre* mice with conditional knockdown of A_1Rs in *Vgat*$^{+}$ INs (SDH-Vgat^{+} IN–A_1R cKD) and their controls (Control; *Vgat-Cre* mice with intra-SDH injection of AAV-FLEx[mCherry]). (I) Percentage of mCherry^{+} (Vgat^{+}) SDH neurons whose NA-evoked response was inhibited by CPA (Control, *n* = 10 cells from 8 mice; SDH-Vgat^{+} IN–A_1R cKD, *n* = 8 cells from 5 mice). (J) Expression of hM3Dq (green, detected by HA-tag) in the SDH at 3 weeks after intra-SDH injection of AAV-FLEx[hM3Dq] in *Hes5-CreERT2* mice treated with TAM. Dashed line indicates an outline of the gray matter of SDH. GFAP (magenta, bottom left), SOX9 (magenta, bottom right). Arrowheads indicate HA-tag^{+} astrocytes. Scale bars, 200 μm (top) and 25 μm (bottom). (K and L) Representative traces of sIPSCs (K) and quantitative analysis of their frequency (L) in SG neurons in spinal cord slices from *Hes5-CreERT2*;AAV-hM3Dq mice treated with TAM [Pre and CNO: before and after bath application of CNO (100 μM), respectively] (*n* = 7 cells from 7 mice; Wilcoxon signed-rank test; *$P < 0.05$). (M and N) Representative traces of sIPSCs (M) and quantitative analysis of their frequency (N) in SG neurons in spinal cord slices from *Hes5-CreERT2*;AAV-FLEx[hM3Dq] mice treated with TAM [Pre and CNO: before and after bath application of CNO with CPT (1 μM), respectively] (*n* = 13 cells from 13 mice; Wilcoxon signed-rank test; n.s., not significant). Data represent mean ± SEM. See also Figure S7 and S8.

INs via A_1R-mediated signals is crucial for stress-induced mechanical hypersensitivity. Moreover, we investigated the role of this interaction in stress-induced alteration of somatosensory information processing in the SDH using c-FOS, a neuronal activity marker, and phosphorylated extracellular signal-regulated kinase (pERK), a neuronal nociceptive input marker in superficial SDH neurons[56]. Consistent with the results of a previous report[57], Aβ fiber stimulation of the hindpaw alone did not increase the number of c-FOS$^+$ (Figure 4, E and F) and pERK$^+$ neurons (Figure 4, G and H) in the superficial SDH (laminae I–IIi using isolectin B4 [IB4], a marker of lamina IIi). Similarly, acute restraint stress alone did not change the number of c-FOS$^+$ and pERK$^+$ neurons (Figure 4, E–H). Interestingly, Aβ fiber stimulation following acute restraint stress exposure significantly increased the number of c-FOS$^+$ and pERK$^+$ neurons in the superficial SDH (Figure 4, E–H). Intrathecal injection of CPT prevented the stress-induced increase in c-FOS$^+$ and pERK$^+$ neurons (Figure 4, E–H). These results suggest that the abnormal responsiveness of superficial SDH neurons to signals from Aβ fibers in mice with acute restraint stress, involves adenosine signals that are important for negatively controlling Vgat$^+$ INs by NA-stimulated Hes5$^+$ astrocytes and for mechanical hypersensitivity.

Discussion

External and internal stressors elicit a variety of biological responses including pain modulation. Acute exposure to a stressor inhibits or facilitates behavioral responses to thermal and mechanical stimuli applied to the skin[33,38,58]. While the mechanism underlying pain inhibition has been studied[33], the neural basis of pain facilitation by stress remains poorly understood. In this study, we identified a circuit, the descending LC$^{\rightarrow SDH}$-NA neurons, that is activated by acute restraint stress exposure and demonstrated that the circuit is necessary for stress-induced mechanical pain hypersensitivity. A notable finding of this study was that Hes5$^+$ astrocytes, a subpopulation of spinal cord astrocytes[22], are the primary target of NA released from descending LC$^{\rightarrow SDH}$-NA neurons for mechanical pain hypersensitivity caused by stress. Thus, this top-down signaling pathway from LC$^{\rightarrow SDH}$-NA neurons to Hes5$^+$ SDH astrocytes is an essential link between stress and mechanical pain sensitization.

Spinal NA derived from LC-NA neurons has been classically implicated in pain inhibitory control[9–11]. The suggested mechanism to this effect is its action on SDH-INs via α_{1A}Rs[9,16]. In contrast, recent our study has unveiled another facet of spinal NA signaling, which is pronociceptive, by identifying Hes5$^+$ astrocytes in the SDH[22]. Mechanistically, spinal NA acts on α_{1A}Rs expressed on Hes5$^+$ astrocytes, increases intracellular Ca^{2+} levels via a G_q/PLC/IP_3 pathway, and causes mechanical hypersensitivity via release of D-serine[22], an activator of NMDA receptors. This study showed that the optogenetic activation of LC$^{\rightarrow SDH}$-NA neurons produced mechanical hypersensitivity via α_{1A}Rs in SDH-Hes5$^+$ astrocytes, indicating the pronociceptive effect of LC$^{\rightarrow SDH}$-NAergic signaling. In contrast, it has also been reported that a similar opto- or chemogenetic activation produces an antinociceptive effect on thermal stimuli[59,60]. The reason for these differing behavioral outcomes remains unclear; however, the stimulus modality used for the behavioral assay (mechanical vs. thermal) may be responsible, since the SDH circuits for mechanical and thermal information processing have been shown to be distinct[3,61–64]. Alternatively, the degree of LC$^{\rightarrow SDH}$-NA neuronal activity may also be involved. Although direct comparisons between studies reporting pro- and anti-nociceptive effects are difficult, our previous studies demonstrated that intrathecal administration of high doses of NA in naïve mice does not induce mechanical pain hypersensitivity and produces an antinociceptive effect on noxious heat[22,16]. Indeed, a continuous stimulation of descending LC-NA neurons over several minutes has been reported to produce antinociceptive effect[65]. Collectively, these findings indicate that the role of LC$^{\rightarrow SDH}$-NA neurons in modulating nociceptive signaling in the SDH is more complex than previously appreciated, and these differences may be related to LC$^{\rightarrow SDH}$-NA neuron activity, NA levels in the SDH, and the differential responses of SDH neurons in the superficial versus deeper laminae.

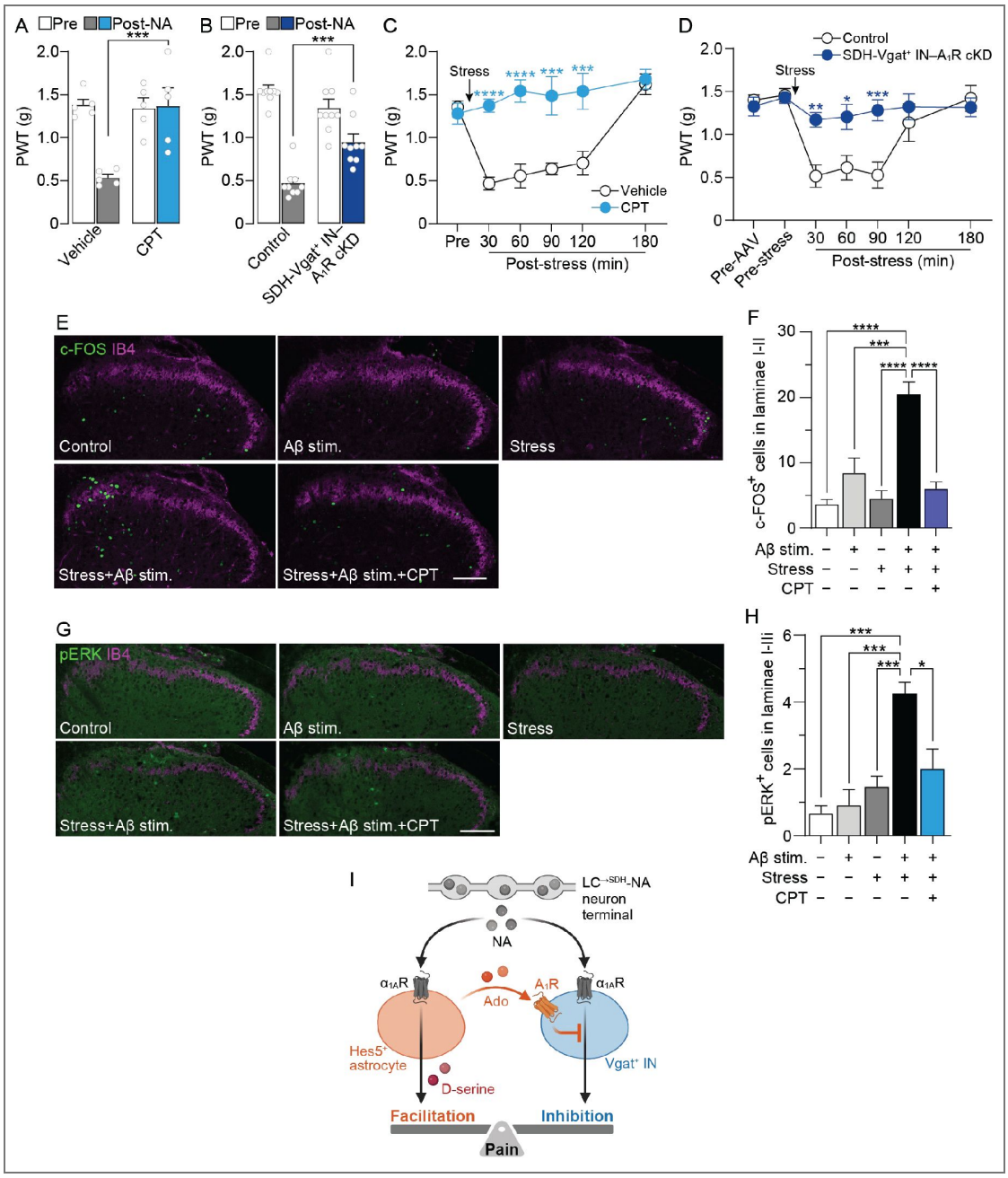

Figure 4. Hes5$^+$ astrocyte-mediated inhibitory signals to SDH-Vgat$^+$ INs contribute to stress-induced mechanical hypersensitivity.

(A and B) PWT before and 30 min after intrathecal administration of NA (0.1 nmol) in wild-type mice pretreated intrathecally with vehicle or CPT (3 nmol) (A: n = 5 mice per group) or in control (*Vgat-Cre* mice with intra-SDH of AAV-FLEx[mCherry]) and SDH-Vgat$^+$ IN–A_1R cKD mice (B: n = 9 mice per group) (two-way ANOVA with post hoc Bonferroni's multiple comparisons test; ***P < 0.001). (C and D) PWT before and after acute restraint stress in wild-type mice pretreated intrathecally with vehicle or CPT (C: Vehicle, n = 6 mice; CPT, n = 5 mice) or in control (*Vgat-Cre* mice with intra-SDH of AAV-FLEx[mCherry]) and SDH-Vgat$^+$ IN–A_1R cKD mice (D: Control, n = 6 mice; SDH-Vgat$^+$ IN–A_1R cKD, n = 7 mice) (two-way ANOVA with post hoc Bonferroni's multiple comparisons test; *P < 0.05, **P < 0.01, ***P < 0.001, ****P <0.0001 vs. vehicle or control group). (E–H) Representative images of c-FOS (green, E), pERK (green, G) and IB4 (magenta, E and G) immunofluorescence in the SDH with or without Aβ fiber stimulation and/or restraint stress. CPT was intrathecally administered 30 min before stress exposure. Quantitative analysis of the number of c-FOS$^+$ (F) and pERK$^+$ (H) cells in superficial laminae of the SDH in each group (n = 4–5 mice per group; one-way ANOVA with post hoc Tukey's multiple comparisons test; *P < 0.05, ***P < 0.001, ****P < 0.0001). (I) Schematic illustration of the mechanisms of stress-induced mechanical pain facilitation highlighting NA signals from LC$^{\rightarrow SDH}$-NAergic terminals to Hes5$^+$ astrocytes and Vgat$^+$ INs. Data represent mean ± SEM. Created with *BioRender.com*.

Given that SDH-INs also express α_{1A}Rs[13,14], it is unclear why pain hypersensitivity is the preferentially manifested behavioral phenotype after activation of $LC^{\rightarrow SDH}$-NAergic signal. This study showed that NA-stimulated $Hes5^+$ astrocytes negatively regulate the activity of SDH-$Vgat^+$ INs. This astrocytic attenuation of SDH-$Vgat^+$ IN activity may involve adenosine signaling because A_1R cKD in SDH-$Vgat^+$ INs canceled the suppressive effect of A_1R agonist on NA-induced enhancement of $Vgat^+$-IN activity and NA-induced mechanical hypersensitivity. The adenosine-mediated inhibition of SDH-INs is consistent with the data from a previous study[47]. In addition, we also found that knockdown of A_1Rs in $Vgat^+$ neurons tended to increase the proportion of $Vgat^+$ neurons with NA-induced depolarizing responses (Figure S8). Thus, these results suggest that spinal NA acts on α_{1A}Rs expressed by both $Hes5^+$ astrocytes and $Vgat^+$ INs; however, NA-stimulated $Hes5^+$ astrocytes suppress $Vgat^+$ IN activity by adenosine signaling via A_1Rs; this induces a state where the $Hes5^+$ astrocyte-derived pain-facilitating effect predominates, causing mechanical pain hypersensitivity (Figure 4I).

While a neuronal model for gating peripherally derived sensory signals in the SDH has been previously established by identifying several subpopulations of INs[1–5], our study proposes a new regulatory mechanism in this model in which $Hes5^+$ astrocytes act as non-neuronal gating cells in the SDH for brain-derived NAergic signaling. This astrocytic gating control of INs may affect processing and transmission of somatosensory information in the SDH. Indeed, a pharmacological blockade of the adenosine signal to SDH-$Vgat^+$ INs suppressed the Aβ fiber-mediated c-FOS and pERK expression in the superficial SDH of stressed mice.

$Preproenkephalin^+$ IN population may be among the SDH-$Vgat^+$ INs involved in stress-induced pain modulation[35]. Interfering with GABA/glycine signaling in the SDH results in abnormal synaptic inputs from primary afferent Aβ fibers onto superficial SDH neurons[66]. Our view is also supported by previous findings from *in vivo* patch-clamp recordings, which show that, in about a half of SG neurons tested, NA enhances excitatory synaptic responses evoked by tactile stimuli (air puff to the skin)[67]. α_{1A}R expression has been reported to be detected in DRG neurons, but its level seems to be much lower than in the spinal cord[68], and primary afferent glutamatergic synaptic transmission has been shown to be unaffected by α_{1A}R agonists[69,70]. Additionally, our hypothesis that $Hes5^+$ astrocytes co-release D-serine and ATP/adenosine in response to α_{1A}R activation by NA is supported by previous findings in the neocortex[71]. Aβ fiber inputs into neurokinin 1 receptor-positive projection neurons in SDH lamina I following inhibition of GABA/glycine signaling is canceled by a pharmacological blockade of NMDA receptors[66], supporting our data that the stress-induced mechanical hypersensitivity was suppressed by the antagonist of D-serine site of NMDA receptors DCK. However, we cannot exclude the possibility that D-serine also acts on NMDA receptors expressed by $Vgat^+$ INs. Nevertheless, given that intrathecal injection of D-serine in naïve mice induces mechanical pain hypersensitivity[22], it appears that the pronociceptive effect of D-serine in the SDH is primarily associated with enhanced pain processing and transmission, presumably via NMDA receptors on excitatory neurons. In addition, the effect of astrocytic adenosine on spinal pain processing has been controversial: both, pronociceptive (consistent with our findings)[47] and antinociceptive[72]. Such different effects might be related in part to the regionally restricted astrocytic subpopulations and factors for their activation. Pro- and anti-nociceptive effects have been reported to be mediated by astrocytes located in superficial and deeper laminae and stimulated by NA (via G protein-coupled α_{1A}Rs)[22] and ATP (via ionotropic P2X7 receptors)[72], respectively. In particular, the regional differences in the role of astrocytes has been demonstrated by our previous study in which a selective chemogenetic stimulation of astrocytes in deeper SDH did not cause mechanical hypersensitivity[22]. Thus, it is conceivable that locally released adenosine from NA-stimulated $Hes5^+$ astrocytes, following acute restraint stress, may suppress SDH-$Vgat^+$ IN function, which results in mechanical pain hypersensitivity. A highly localized adenosine release from $Hes5^+$ astrocytes and the spatially restricted neuron–astrocyte communication via adenosine signaling need to be investigated in future studies.

In this study, we showed mechanical hypersensitivity by acute exposure to restraint stress and investigated its mechanisms; however, there are also many studies reporting acute stress-induced antinociception (Table S1). A precise explanation for the bidirectional outcomes remains elusive.

However, it is widely recognized that the extent and direction of pain modulation may be due to several factors, including the nature, duration, and intensity of the stressor, as well as the sensory modality assessed in behavioral tests[33,34]. In fact, most studies reporting antinociceptive effects of acute restraint stress assessed behavioral responses to heat stimuli (Table S1). This observation is consistent with the findings in our previous study[16] and the present study (Figure S2). In contrast to the robust and consistent antinociceptive effects observed with thermal stimuli, some studies evaluating behavioral responses to mechanical stimuli have reported stress-induced hypersensitivity[38] (Table S1), which aligns with our current findings. Nevertheless, acute and short-term exposure (≤1 hour) to restraint stress induces mechanical pain hypersensitivity, which was not observed with longer exposure (2 hours) (Figure S1) (although a 2-hour restraint stress exposure suppresses behavioral response to nociceptive thermal stimuli[16]). Thus, descending $LC^{\rightarrow SDH}$-NA neurons, $Hes5^{+}$ SDH astrocytes, or their output signals involved in modulating mechanical pain behavior may be attenuated by unidentified inhibitory signals evoked by longer exposure to restraint stress. A similar bidirectional behavioral outcome on mechanical pain has also been observed with intrathecal NA; low doses of NA induce mechanical pain hypersensitivity while higher doses do not[22]. Thus, the bidirectional change may depend on the level of NA neuronal activity and NA content in the SDH, which is supported by a previous report[73].

Clinically, stressor-evoked psychological and physical responses are considered critical for the development of chronic pain[36], especially nociplastic pain, a condition that arises from altered nociceptive signaling without actual or threatened tissue damage, or disease or lesion of the somatosensory system[37]. In fact, patients with chronic pain have a high incidence of stress-related psychiatric disorders, such as anxiety, fear, and depression[11,74]; stressful life events are known to be a key factor in establishing fibromyalgia and enhance pain in patients with irritable bowel syndrome and headaches[37]. Thus, our findings provide a mechanistic insight into the link between stress and pain modulation and may help in understanding and developing a new strategy for chronic pain, including nociplastic pain.

There are several limitations to this study. First, under our experimental conditions, where AAV vectors were injected into both the LC and SDH (L4) to express genes in $LC^{\rightarrow SDH}$ neurons, only a small proportion (4.4%) of all LC-NA neurons could be manipulated (Figure 1, I–K; Figure S4, B and C), although we confirmed specific expression of DTRs in NA neurons within the LC, but not in A5 or A7 (Figure S4A). This low proportion is likely due to the selective targeting of LC-NA neurons that project to the L4 segment of the SDH. The total number of SDH-projecting LC-NA neurons across all spinal segments may be much higher. Given that primary afferent sensory fibers from the plantar skin of the hindpaw predominantly terminate in the L4 segment of the SDH, it is plausible that ablation of even a relatively small number of NA neurons in the LC can have a significant impact on behavior. Second, in our model (Figure 4I), we proposed that NA released by $LC^{\rightarrow SDH}$ NA neurons inhibits SDH-INs. Although we demonstrated that optogenetic stimulation of $LC^{\rightarrow SDH}$ NA terminals in the SDH induces endogenous NA release, we were unable to determine whether the released NA modulates the function of $Hes5^{+}$ astrocytes and $Vgat^{+}$ INs, or their interactions. Addressing this question would require the use of *Vgat-Cre* and/or *Hes5-CreERT2* mice; however, employing these lines precludes the use of *NET-Cre* mice, which are essential for specific and efficient expression of ChrimsonR in $LC^{\rightarrow SDH}$ NA neurons. Third, in our in vivo optogenetic experiments showing that stimulation of $LC^{\rightarrow SDH}$-NAergic terminals in the SDH causes mechanical pain hypersensitivity (Figure 1N), light could reach only the superficial laminae, even though ChrimsonR expression in $LC^{\rightarrow SDH}$-NAergic terminals was also observed in both superficial and deeper laminae of the SDH (Figure S6). Kucharczyk et al. have reported that NA released from descending pathways reduces activity of wide-dynamic-range neurons in deeper laminae[65]. Therefore, the roles of NA signaling in superficial versus deeper laminae should also be further investigated.

An important future subject is to clarify the discrepancy for the pro- and antinociceptive role of $LC^{\rightarrow SDH}$-NAergic signaling in the SDH. Since one possible candidate could be related to the sensory modality used for behavioral testing, other assays (e.g., Randall-Selitto test, CatWalk gait analysis, and weight-bearing test) should be tested. Furthermore, a difference between the duration of

behavioral responses and Ca^{2+} events after acute restraint stress should also be addressed in further investigation. The behavioral effect of stress on PWT (Figure 1E) persisted for 120 min after stress exposure, whereas Ca^{2+} events changes were only observed during stress exposure (Figure 1B). A similar temporal difference is also observed following intraplantar injection of capsaicin[22]; while $LC^{\rightarrow SDH}$-NA neuron-mediated astrocytic Ca^{2+} responses in SDH astrocytes last for 5–10 min after injection, behavioral hypersensitivity peaks around 60 min post-injection and gradually returns to baseline over the subsequent 60–120 min. These findings raise the possibility that astrocyte-mediated mechanical pain hypersensitivity in the SDH may involve a sustained alteration in spinal neural function, such as central sensitization.

Methods

Animals

Male C57BL/6J mice (CLEA Japan), male and female *NET-Cre* mice [Tg(*Slc6a2-cre*)#Stl] (kindly provided by Prof. Thomas McHugh, RIKEN Center for Brain Science)[41], *Hes5-CreERT2* mice [Tg(*Hes5-cre/ERT2*)2Vtlr] (kindly provided by Prof. Verdon Taylor)[75], *Adra1a*$^{flox/flox}$ mice[22], *Vgat-Ires-Cre* mice [*Slc32a1*$^{tm2(cre)Lowl}$/J] (Stock No: 016962, The Jackson Laboratory)[76], and *Rosa26-tdTomato* mice [B6.Cg-*Gt(ROSA)26Sor*$^{tm14(CAG-tdTomato)Hze}$/J] (Stock No: 007914, The Jackson Laboratory)[77] were used. To generate *Hes5-CreERT2*;*Adra1a*$^{flox/flox}$ mice[22] or *Vgat-Cre*;*Adra1a*$^{flox/flox}$ mice[16], *Adra1a*$^{flox/flox}$ mice were crossed with *Hes5-CreERT2* mice or *Vgat-Ires-Cre* (*Vgat-Cre*) mice, and the obtained *Hes5-CreERT2*;*Adra1a*$^{flox/+}$ mice or *Vgat-Cre*;*Adra1a*$^{flox/+}$ mice were further crossed with *Adra1a*$^{flox/flox}$ mice. Cre-negative *Adra1a*$^{flox/flox}$ littermate mice were used as controls. For induction of CreERT2 recombinase activity, *Hes5-CreERT2* mice were given an intraperitoneal (i.p.) injection of tamoxifen (#T5648, Sigma-Aldrich; 2 mg dissolved in 100 µl corn oil [#032-17016; Wako, Saitama, Japan]) once a day for 5–10 successive days. We used tamoxifen-injected mice for further analyses 7 days or more after the last injection. All mice used were 8–12 weeks of age at the start of each experiment and were housed at temperature and humidity ranges of 21–23°C and 40–60%, respectively, with a 12-hour light-dark cycle. All animals were fed food and water ad libitum. All animals were housed in standard polycarbonate cages in groups of same-sex littermates. All animal experiments were conducted according to relevant national and international guidelines contained in the 'Act on Welfare and Management of Animals' (Ministry of Environment of Japan) and 'Regulation of Laboratory Animals' (Kyushu University) and under the protocols approved by the Institutional Animal Care and Use committee review panels at Kyushu University.

Restraint stress model

According to the methods described in our previous study[16], mice were restrained by placing them in a Falcon® 50-ml conical tube (#352070; Corning) with a hole in the tip. The space remaining behind the mouse was filled with a paper towel. Mice were allowed to breathe but not turn around. Control mice were handled briefly and placed in home cages without water or food for 1 hour.

Measurement of behavioral response to mechanical stimuli using von Frey filaments

Mice were placed individually in an opaque plastic cylinder, which was placed on a wire mesh, and habituated for 0.5–1 hour to allow acclimatization to the new environment. After that, calibrated von Frey filaments (0.02–2.0 g; #NC12775; North Coast Medical) were applied to the plantar surface of the hindpaw of mice from below the mesh floor. 50% paw withdrawal threshold was calculated using the up-down method[78]. The basal mechanical threshold was determined by performing von Frey test before restraint stress exposure, AAV microinjection, DTX administration, optogenetic stimulation, intrathecal injection of several drugs and tamoxifen administration. Mechanical sensitivity was evaluated at 30, 60, 90, 120 and 180 min after restraint stress or optogenetic stimulation, or at 30 min after intrathecal injection of NA or Phe.

Measurement of behavioral response to thermal stimuli in hot-plate and paw-flick tests

For the hot-plate test (HOT/COLD PLATE ANALGESIA METER, MK-350HC, Muromachi Kikai, Tokyo, Japan), the latency to exhibit nociceptive behaviors (licking or jumping) in response to thermal stimulation (50°C)[16,79] was recorded. To prevent tissue damage, a cut-off time was set at 60 sec. For the paw-flick test (Tail Flick Unit, 7360, Ugo Basile, Gemonio, Italy), the latency to elicit nociceptive responses (paw withdrawal) against heat stimulation at 40 V[22] was recorded, with a cut-off time of 10 sec to avoid tissue damage.

Measurement of behavioral response to motor function by Rotarod test

Before AAV injection, each mouse was trained on a rotarod (3[cm diameter, 8[r.p.m.; Rotarod, KN-75, Natsume Seisakusho, Tokyo, Japan) until it could remain on the apparatus for 60[sec without falling[80]. The mice then underwent a 60-s rotarod test both before and after DTX administration.

Recombinant AAV (rAAV) vector production

pAAV-CAG-FLEx[GCaMP6s]-WPRE (#100842) and pAAV-synapsin (Syn)-FLEx[ChrimsonR-tdTomato]-WPRE (#62723) were purchased from Addgene. The genes encoding GCaMP6m (#40754; Addgene), Cre, $GRAB_{NE1m}$ (#123308; Addgene) and mCherry were subcloned into the pENTR plasmid (Thermo Fisher Scientific). To produce AAV vectors, we inserted GCaMP6m, $GRAB_{NE1m}$ and mCherry into pZac2.1-gfaABC$_1$D-WPRE plasmid and Cre into pZac2.1-enhanced synapsin (ESYN)-WPRE plasmid. To produce the AAV vector for the Cre-switch system, vectors containing the promoters encoding EF1α were generated from pAAV-CA-FLEx (#38042; Addgene) by substituting the promoter. We then inserted AcGFP, DTR-EGFP (kindly provided by Prof. Kenji Kohno, Nara Institute of Science and Technology), mCherry and hM3Dq (#45547; Addgene) into pAAV-EF1α-FLEx. The genes encoding U6-sgRNA (#61593; Addgene) and SaCas9 (#78601; Addgene) were subcloned into the pENTR plasmid. Synthetic oligonucleotides including the targeting sequence for *Adora1* (5'-AAGTTCCGGGTCACCTTTCTG-3') and non-targeting sequence (5'-CCATGTGA TCGCGCTTCTCGT-3') were replaced with the targeting site in the original pENTR-U6-sgBsa1 plasmid. The resulting U6-sgRNA cassette was transferred into pAAV-CMV-FLEx[mCherry]-WPRE plasmid to generate pAAV-CMV-FLEx[mCherry]-WPRE-U6-sgAdora1/sgYFP (sgControl). The SaCas9 cassette was transferred into pAAV-CMV-FLEx-WPRE plasmid to generate pAAV-CMV-FLEx[SaCas9]-WPRE. rAAV vectors were produced from human embryonic kidney 293T (HEK293T) cells with triple transfection [pZac or pAAV, cis plasmid; pAAV2/5 (University of Pennsylvania Gene Therapy Program Vector Core), pAAV2/9 (University of Pennsylvania Gene Therapy Program Vector Core) or pAAV2/retro (#81070; Addgene), trans plasmid; pAd DeltaF6, adenoviral helper plasmid (University of Pennsylvania Gene Therapy Program Vector Core)] and purified by two cesium chloride density gradient purification steps. The vector was dialyzed against phosphate-buffered saline (PBS) containing 0.001% (v/v) Pluronic-F68 (#24040032; Thermo Fisher Scientific) using Vivaspin Turbo 15 100,000 MWCO (#VS15T41; Sartorius). The genome titer of rAAV was determined by Pico Green fluorometric reagent (#P7589; Thermo Fisher Scientific) following denaturation of the AAV particles. Vector were stored at −80°C until use.

Intra-SDH and intra-LC injection of rAAV vectors

Viral vector injection was performed in accordance with our previously described method[22,81]. Mice were deeply anesthetized by subcutaneous injection of ketamine (100 mg/kg) and xylazine (10 mg/kg). For intra-SDH injection, the skin was incised at Th11–L4 vertebrae, and custom-made clamps were attached to the caudal sites of the vertebral column. Paraspinal muscles around the left side of the interspace between Th13 and L1 vertebrae were removed, and the dura mater and arachnoid membrane were carefully incised using the tip of a 30-G needle to make a small window allowing a glass microcapillary to insert directly into the SDH. The microcapillary was inserted into the unilateral SDH (around 120–150 μm in depth from the surface of the dorsal root

entry zone). rAAV solutions (approximately 500 nl) were injected using a Micro4 Micro Syringe Pump Controller (World Precision Instrument). After microinjection, the glass microcapillary was removed, the skin was sutured with 5-0 silk, and the mice were kept on a heating pad until recovery. For intra-LC injection, rAAV solutions were injected (approximately 300 nl in one site) adjacent to the LC (anteroposterior (AP): −5.4 mm from the bregma; mediolateral (ML): ±0.9 mm; dorsoventral (DV): −3.2 mm from the dura). Only AAV2/9-CAG-FLEx[GCaMP6s]-WPRE was injected unilaterally, and the other AAV vectors were injected bilaterally. To keep the bregma and lambda in the same horizontal plane, tolerance was maintained at <50 μm in the dorsoventral axis between the bregma/lambda. The microcapillary was withdrawn 3 min after ending the injection. The skin was then sutured with 5-0 silk, and the mice were kept on a heating pad until recovery. We used virus-injected mice for further analyses 3 weeks or more after the last injection. The following viral titers were used: AAV2/9-CAG-FLEx[GCaMP6s]-WPRE, AAV2/9-gfaABC$_1$D-GCaMP6m-WPRE, AAV2/9-EF1α-FLEx[AcGFP]-WPRE (for *NET-Cre* mice), AAV2/9-EF1α-FLEx[DTR-EGFP]-WPRE (for *NET-Cre* mice), AAV2/9-EF1α-FLEx[mCherry], AAV2/9-hSyn-FLEx[ChrimsonR-tdTomato], AAV2/9-gfaABC$_1$D-GRAB$_{NE1m}$-WPRE, AAV2/5-EF1α-FLEx[hM3Dq], AAV2/9-CMV-FLEx[SaCas9]-WPRE and AAV2/5-gfaABC$_1$D-mCherry: 1.0×10^{12} genome copies (GC)/ml; AAV2/retro-ESYN-Cre-WPRE: 3.0×10^{12} GC/ml; AAV2/9-EF1α-FLEx[AcGFP]-WPRE (for WT mice) and AAV2/9-EF1α-FLEx[DTR-EGFP]-WPRE (for WT mice): 2.0×10^{12} GC/ml; AAV2/9-CMV-FLEx[mCherry]-WPRE-U6-sgYFP and AAV2/9-CMV-FLEx[mCherry]-WPRE-U6-sgAdora1: 0.5×10^{12} GC/ml.

Immunohistochemistry

Mice were deeply anesthetized with an i.p. injection of pentobarbital and transcardially perfused with PBS (#041-20211; Wako, Saitama, Japan) followed by ice-cold 4% paraformaldehyde (PFA; #162-16065; Wako, Saitama, Japan)/PBS. The transverse L4 segments of the spinal cord and brain were removed, postfixed in the same fixative for 3 hours (spinal cord) or overnight (brain) at 4°C, and placed in 30% sucrose solution for 24–48 hours at 4°C. After incubation, the tissues were embedded in OCT compound (#4583; Sakura Finetek Japan, Osaka, Japan) and stored at −25°C before use. Transverse spinal cord and brain sections (30 μm) were incubated in blocking solution (3% normal goat serum [#S-1000; Vector Laboratories] or normal donkey serum [#017-000-121; Jackson ImmunoResearch]) for 2 hours at room temperature and then incubated for 48 hours at 4°C with primary antibodies: polyclonal rabbit anti-tyrosine hydroxylase (TH; 1:1000; #AB152; Millipore); polyclonal sheep anti-TH (1:1000; #AB1542; Millipore); monoclonal mouse anti-noradrenaline transporter (NET; 1:2000; #NET05-2; Mab Technologies); polyclonal rabbit anti-green fluorescent protein (GFP; 1:1000; #598; MBL International); monoclonal rabbit anti-hemagglutinin (HA)-tag (1:1000; #3724; Cell Signaling); monoclonal rat anti-glial fibrillary acidic protein (GFAP; 1:2000; #13-0300; Invitrogen); polyclonal goat anti-SRY-related high-mobility group box 9 (SOX9; 1:1000; # AF3075; R&D Systems); polyclonal goat anti-paired box 2 (PAX2; 1:500; # AF3364; R&D Systems); monoclonal rat anti-mCherry (1:2000; #M11217; Thermo Fisher Scientific); polyclonal rabbit anti-phospho-p44/42 MAPK (ERK1/2) (Thr202/Tyr204) (pERK; 1:500; #9101; Cell Signaling); anti-isolectin B4 (IB4)-biotin conjugate (1:1000; # I21414; Thermo Fisher Scientific); monoclonal rabbit anti-c-FOS (1:5000; #226 008; Synaptic systems). After incubation, tissue sections were washed and incubated for 3 hours at room temperature with secondary antibodies (Alexa Fluor™ 488, 546 and/or 555; #A11001, A11008, A11035, A11056, A11081, S32351; Thermo Fisher Scientific: #ab150178; Abcam: DyLight™ 405; #705-475-147; Jackson ImmunoResearch). Then, tissue sections were washed, slide mounted, and subsequently placed under coverslips with VECTASHIELD Hardmount (Vector Laboratories). Immunofluorescence images were obtained with confocal laser microscopy (#LSM700 or LSM900; Carl Zeiss).

Fiber photometry

Immediately after microinjection of AAV vectors encoding GCaMPs, the mice were implanted with an optic cannula. Cannulae were purchased from RWD (#R-FOC-BL400C-50NA, ø1.25 mm ferrule, ø400 μm optic fiber, 0.50 NA). The length of the optic fiber protruding from the tip of the ferrule was 4.0 mm. Optic cannula was implanted in the unilateral LC (AP: −5.4 mm from the bregma; ML: 0.9 mm; DV: −3.0 mm from the dura). Next, the cannula was secured using two types of dental

glues (Super-bond; Sun Medical, Shiga, Japan: UNIFAST III; GC, Tokyo, Japan). After implantation, the skin was sutured with 5-0 silk, and the mice were kept on a heating pad until recovery. We used cannula-implanted mice for fiber photometry 3 weeks or more after the surgery, and monitored Ca^{2+} events in LC-NA neurons during restraint stress using the conical tube with a narrow slit (Movie). GCaMP fluorescent signals were obtained with the fiber photometry apparatus from Doric Lenses, which includes a fiber photometry console (FPC_V6), a 415-nm LED illumination (CLED_415), a 465-nm LED illumination (CLED_465), an LED driver (LEDD_2), and a fluorescence mini cube with built-in fluorescence photodetector amplifier (iFMC4-G2_IE(410-420)_E(460–490)_F(500–550)_S). A 415-nm light was modulated at 208[Hz, while a 465-nm light was modulated at 572[Hz. The optic cannula implanted in mice and fluorescence mini cube were connected by a low-autofluorescence patch cable (#MAF1L1; Thorlabs). The power output at the fiber tip was 30– 40[μW. After connecting to the patch cable, the mice were allowed to move freely in the home cage for at least 10 min for habituation. After habituation, fluorescence recording was started. Emitted signals from the tissue were collected through the same fiber and sampled at 12 kHz.

Processing and analysis of fiber photometry data

To avoid the effects of photobleaching, data from the first 5 min of recording were discarded. The raw data were then decimated to 30[Hz (down-sampled by 400) and low-pass Butterworth-filtered at 2[Hz. The 415-nm excitation channel served as an isosbestic, Ca^{2+}-independent control wavelength for GCaMP, allowing for bleaching and movement artifact corrections when directly fitted to the Ca^{2+}-dependent 465-nm channel. The Correction Baseline function from Doric Neuroscience Studio (Doric Lenses) was used to fit the 415-nm signal to the 465-nm signal using an adaptive iterative re-weighted Penalized Least Squares algorithm[82]. The fluorescence change was expressed as a relative change, $\Delta F/F = (F_{465}-F_{415})/F_{415}$, where F_{465} is the 465 nm-induced Ca^{2+}-dependent signal, and F_{415} is the 415 nm-induced Ca^{2+}-independent signal. During restraint stress, the Ca^{2+} transients and escape behaviors (struggling) occurred almost simultaneously (Movie), but the 415 nm-induced Ca^{2+}-independent signals was unchanged. Robust Z-scores were then calculated as $Z = (\Delta F/F - \text{Median } \Delta F/F)/\text{NIQR}$, where Median $\Delta F/F$ is the median of $\Delta F/F$ during the entire measurement period, and NIQR is the normalized interquartile range (0.7413 × interquartile range). Ca^{2+} events were detected with a threshold of Z-score >3. The frequency of Ca^{2+} events was calculated as the number of Ca^{2+} events per minute in the 10 min before stress, 60 min during stress (10 min × 6 times), and 10 min after stress.

Drug administration

To ablate DTR^{+} neurons, DTX (10 μg/kg in PBS; #048-34371; Wako, Saitama, Japan) was administered i.p. for two successive days 3 weeks after intra-LC injection of AAV2/9-EF1α-FLEx[DTR-EGFP] or [AcGFP]-WPRE. We used DTX-injected mice for further analyses 2 weeks or more after the last injection. For intrathecal injection, a 30-G needle attached to a Hamilton microsyringe was inserted between the L5/L6 vertebrae and then punctured through the dura. The following drugs and doses were used for intrathecal injection experiments: silodosin (3 nmol in 5 μl PBS; #191-17591; Wako, Saitama, Japan; injection was given 30 min before optogenetic stimulation); L-norepinephrine hydrochloride (0.1 nmol in 5 μl saline; #74480; Sigma-Aldrich); 5,7-dichlorokynurenic acid (DCK; 10 nmol in 5 μl saline of 2% dimethylsulfoxide (DMSO); #0286; Tocris; injection was given immediately before the start of exposure to restraint stress); (R)-(-)-phenylephrine hydrochloride (Phe; 0.05 nmol in 5 μl saline; #163-11791; Wako, Saitama, Japan); 8-cyclopentyl-1,3-dimethylxanthine (CPT; 3 nmol in 5 μl saline of 2% DMSO; #C102; Sigma-Aldrich; injection was given immediately before the start of exposure to restraint stress or 30 min before intrathecal injection of NA).

In vivo optogenetic stimulation

Immediately after microinjection of AAV vectors encoding ChrimsonR, mice were implanted with an optic cannula. A cannula comprised a ceramic ferrule (#CFLC230-10; Thorlabs; ø1.25 mm, 6.4 mm length) and an optic fiber (#FT200UMT; Thorlabs; ø200 µm, 0.39 NA). The length of the optic fiber protruding from the tip of the ferrule was less than 0.3 mm. The vertebrae were immobilized in place using a metal bar along the Th12–L1. A small laminectomy was performed through the Th13 bone using a dental drill. The cannula was secured above the dura mater using two types of dental glues (Super-bond; Sun Medical: UNIFAST III; GC). In this procedure, the dura mater and spinal cord parenchyma were left intact and unscathed. After implantation, the skin was sutured with 5-0 silk, and the mice were kept on a heating pad until recovery. We used cannula-implanted mice for optogenetic stimulation 3 weeks or more after the surgery. To activate ChrimsonR in $LC^{\rightarrow SDH}$-NA axons/terminals, 625-nm LED light (#M625F2; Thorlabs) was delivered through a ferrule patch cable (#M83L01; Thorlabs). Light stimulations (2 mW, 10 Hz, 5-ms pulse duration, 5-s light on, 15-s light off, 10 cycles) were generated by an LED driver (#LEDD_2; Doric Lenses).

Fluorescent Ca^{2+} and NA imaging in spinal cord slices

Fluorescent imaging was performed in accordance with our previously described method[22]. GCaMP6m- and $GRAB_{NE1m}$-expressing mice were anesthetized with an i.p. injection of urethane (1.2–1.5 mg/kg), and lumbosacral laminectomy was performed. The spinal cord (L1–S2) was removed and placed in a cold, high-sucrose, artificial cerebrospinal (aCSF) fluid (27 mM $NaHCO_3$, 1.4 mM NaH_2PO_4, 2.5 mM KCl, 7.0 mM $MgSO_4$, 1.0 mM $CaCl_2$, 222 mM sucrose, and 0.5 mM ascorbic acid), which was bubbled with 95% O_2 and 5% CO_2. After cutting all ventral and dorsal roots, transverse L4 spinal cord slices (350 µm thick) were made using a vibrating microtome (#VT1200; Leica); the slices were kept in oxygenated aCSF solution (125 mM NaCl, 1.25 mM NaH_2PO_4, 2.5 mM KCl, 1.0 mM $MgCl_2$, 2.0 mM $CaCl_2$, 26 mM $NaHCO_3$, and 20 mM glucose) at room temperature (22–25°C) for at least 30 min before use. The slices were placed in a recording chamber, and fluorescent signals were measured using a confocal laser scanning microscope (#FV3000; Olympus, Tokyo, Japan). The chamber was perfused with aCSF saturated with 95% O_2 and 5% CO_2 at 31–32°C and at 2–3 ml/min using peristaltic pumps. A 488-nm diode laser was used for the excitation of GCaMP6m and $GRAB_{NE1m}$. The size of the image was 509 × 509 μm^2 (512 × 512 pixels). The recordings were acquired at a rate of 1.083 s per image. Light stimulations (1 mW, 10 Hz, 5-ms pulse duration, 1–20 s) were generated by an LED driver (#LEDD_2; Doric Lenses) and delivered through an optic fiber (Thorlabs, FT200UMT, ø200 µm, 0.39 NA). For an experiment on $\alpha_{1A}R$ inhibition, optogenetic stimulations (10 s) were performed twice (at least 15-min apart) in the same slice. Silodosin (40 nM in aCSF) was continuously applied by bath application starting 5 min before the onset of 2nd optogenetic stimulation. After optogenetic stimulation, NA (1 or 10 µM in aCSF) was applied by bath application as the positive control.

Processing and analysis of Ca^{2+} and NA imaging data

Videos were imported into ImageJ Fiji (*https://imagej.net/software/fiji/*), and motion artifacts were corrected using TurboReg[83]. The fluorescence change was expressed as a relative percentage change, $\Delta F/F = 100 \times (F_t - F_0)/F_0$, where F_t is the fluorescence at time t, and F_0 is the baseline average for 30 frames before the start of stimulation. For Ca^{2+} imaging using GCaMP, the size of each region of interest (ROI) was set to a circle with a diameter of 10 µm[22]. ROIs were manually identified based on the following criteria: located within 200 µm from the surface of gray matter and ≥30% $\Delta F/F$ fluorescence change after optogenetic stimulation or NA application. For the experiment on $\alpha_{1A}R$ inhibition, normalized $\Delta F/F$ was calculated as ($\Delta F/F$ in 2nd stimulation)/($\Delta F/F$ in 1st stimulation). For NA imaging using $GRAB_{NE1m}$, the raw image was binarized, and a single ROI was detected from such a binarized image with the following parameters: contiguous pixel number >100 and 0[<[circularity[<[1[73]. Calculation of $\Delta F/F$ in ROIs was performed using the Time Series Analyzer V3 plugin in ImageJ.

Whole-cell patch-clamp recordings using spinal cord slices

According to our previously described method[16], mice were deeply anesthetized with urethane (1.2–1.5 mg/kg, i.p.), and the lumbar spinal cord was removed and placed in a cold high-sucrose aCSF (250 mM sucrose, 2.5 mM KCl, 2 mM $CaCl_2$, 2 mM $MgCl_2$, 1.2 mM NaH_2PO_4, 25 mM $NaHCO_3$, and 11 mM glucose). Parasagittal and transverse spinal cord slices (250–300 μm thick) were made with a vibrating microtome (VT1200, Leica) and then the slices kept in oxygenated aCSF solution (125 mM NaCl, 2.5 mM KCl, 2 mM $CaCl_2$, 1 mM $MgCl_2$, 1.25 mM NaH_2PO_4, 26 mM $NaHCO_3$, and 20 mM glucose) at room temperature (22–25°C) for at least 30 min. The spinal cord slice was then put into a recording chamber, where it was continuously superfused with aCSF solution at 25– 28°C at a flow rate of 4–6 ml/min. Recordings were made with the Axopatch 700B amplifier and pCLAMP 10.4 acquisition software (Molecular Devices). Data were digitized with an analog-to-digital converter (Digidata 1550; Molecular Devices), stored on a personal computer with a data acquisition program (ClampeX version 10.4; Molecular Devices), and analyzed with a software package (Clampfit version 10.7; Molecular Devices). Spontaneous inhibitory postsynaptic currents (sIPSCs) were recorded in the voltage-clamp mode at a holding potential of 0 mV. Patch pipettes were filled with an internal solution (120 mM $CsMeSO_4$, 15 mM CsCl, 10 mM HEPES, 5 mM QX-314, 4 mM MgATP, 0.3 mM Na_2GTP, 0.2 mM EGTA, 10 mM TEA-Cl and 8 mM NaCl [pH 7.28] adjusted with CsOH), and whole-cell patch-clamp recordings were made from SG neurons. Resting membrane potentials (RMPs) were recorded in current-clamp mode. Patch pipettes were filled with an internal solution (125 mM K-gluconate, 10 mM KCl, 0.5 mM EGTA, 10 mM HEPES, 4 mM ATP-Mg, 0.3 mM NaGTP, 10 mM phosphocreatine, pH 7.28 adjusted with KOH), and whole-cell patch-clamp recordings were made from tdTomato$^+$ or mCherry$^+$ neurons. The following drugs were used: NA (20 μM; #74480; Sigma-Aldrich), clozapine-N-oxide (CNO; 100 μM; #BML-NS105; Enzo Life Sciences), CPT (1 μM), N6-cyclopentyladenosine (CPA; 1 μM; #119135; Sigma-Aldrich), CNQX disodium salt hydrate (CNQX; 10 μM; #C239; Sigma-Aldrich), (+)-MK-801 hydrogen maleate (MK-801; 20 μM; #M107; Sigma-Aldrich), 1(S), 9(R)-(-)-bicuculline methiodide (10 μM; #14340; Sigma-Aldrich) and strychnine (1 μM; #S0532; Sigma-Aldrich). All drugs were dissolved in aCSF solution. CNO was superfused for 3 min. Bath application of CPT was continuously superfused from 4 min before CNO application. NA was superfused with an antagonist cocktail (CNQX, MK-801, bicuculline and strychnine) for 3–5 min to block synaptic inputs from other neurons to the recorded Vgat$^+$ neurons[48,49]. If the recording neuron was depolarized by NA perfusion, then CPA was co-perfused with NA and an antagonist cocktail for 3 min. The frequency of sIPSCs for 1 min of pre- and post-NA application were quantified using Clampfit version 10.7 (Molecular Devices). We quantified averaged RMP for 1 min of pre- and post-drug application, and a change in RMP (ΔRMP) of 5 mV or more was judged to be depolarization or hyperpolarization.

In situ hybridization

Mice were deeply anesthetized with an i.p. injection of pentobarbital and transcardially perfused with PBS followed by ice-cold 4% PFA/PBS. The L4 spinal cord was removed and postfixed in the same fixative 24 hours at 4°C. After that, tissues were incubated with 10%, 20% and 30% sucrose solutions at 4°C, embedded in OCT compound, and stored at −25°C before use. The L4 segments were sectioned at a thickness of 14 μm. *In situ* hybridization was performed using RNAscope® Multiplex Fluorescent Reagent Kit v2 (#323100; ACDbio), according to the manufacture's protocol for fixed frozen tissue. The following probes were used: Mm-Adora1 (#402261; ACDbio); Mm-Slc32a1-C3 (#319191-C3; ACDbio). Tissue sections were analyzed using an LSM700 Imaging System. Cells were considered positive if three or more punctate dots were present in the nucleus and/or cytoplasm[14].

Electrical stimulation of Aβ fibers and counting of c-FOS$^+$ and pERK$^+$ neurons in the SDH

For pERK immunofluorescence, but not for c-FOS, after exposure to 1-hour restraint stress, mice were deeply anesthetized with an i.p. injection of urethane (1.2–1.5 mg/kg). Thirty min after stress, Aβ fiber stimulation was performed. The electrodes were attached to the plantar and dorsal surfaces of the left hindpaw. Transcutaneous nerve stimuli were applied using a stimulus generator (#STG4002-16[mA; Multi Channel Systems). The current intensity of the 2,000-Hz stimuli was 1,000[μA[57]. Mice were fixed at 2 (for pERK) or 90[min (for c-FOS) after electrical stimulation. For c-FOS immunostaining, mice were deeply anesthetized with an i.p. injection of pentobarbital prior to fixation. For quantification of c-FOS$^+$ and pERK$^+$ cells, three sections from the L4 spinal cord segments were randomly selected from each mouse, and the number of c-FOS$^+$ and pERK$^+$ neurons in the superficial laminae I–IIi (defined by staining of IB4) was counted. Consistent with a previous study[57], we confirmed that electrical stimulation of Aδ and C fibers, but not Aβ fibers, induced ERK phosphorylation in SDH neurons (data not shown).

Statistical analysis

Statistical analyses were performed using Prism (GraphPad). Quantitative data were expressed as the mean ± SEM. Statistical significance of differences was determined by using two-tailed paired *t*-test (Figure S1, S2E and S5), Mann-Whitney test (Figure 2F and S4B), Wilcoxon signed-rank test (Figure 3L, 3N and S7C), Fisher's exact test (Figure S8), Friedman test with Dunn's multiple comparisons test (Figure 1E and 2E), one-way ANOVA with Dunnett's multiple comparisons test (Figure 2C), one-way ANOVA with Tukey's multiple comparisons test (Figure 4F and 4H) and repeated measures two-way ANOVA with Bonferroni's multiple comparisons test (Figure 1B, 1H, 1K, 1N, 2G, 2H, 2I, 2J, 3A, 3B, 3C, 4A, 4B, 4C, 4D, S2E and S5), as appropriate, after determining the normality (Kolmogorov–Smirnov test or Shapiro–Wilk test). P values are indicated as $*P < 0.05$, $**P < 0.01$, $***P < 0.001$, $****P < 0.0001$.

Data availability

All data associated with this study are present in the paper or the Supplemental Information.

Acknowledgements

We would like to thank Editage for editing a draft of this manuscript, and the University of Pennsylvania vector core for providing pZac2.1, pAAV2/5, pAAV2/9 and pAd DeltaF6 plasmid. This work was supported by Japan Society for the Promotion of Science (JSPS) KAKENHI Grants JP19H05658 (M.T.), JP20H05900 (M.T.) and JP24H00067 (M.T.), by the Core Research for Evolutional Science and Technology (CREST) program from AMED under Grant Number 25gm1510013h (M.T.), and by Research Support Project for Life Science and Drug Discovery (Basis for Supporting Innovative Drug Discovery and Life Science Research (BINDS)) from AMED under Grant Number JP25ama121031 (M.T.). R.K-K., S.U., and K.Y. were JSPS research fellows (JP22KJ2471, JP23KJ1729, and JP19J21063, respectively).

Additional information

Author contributions

Conceptualization: MT

Formal analysis: RKK, SU, KY

Funding acquisition: RKK, SU, KY, MT

Investigation: RKK, SU, KY, KK, DK

Methodology: RKK, SU, KY, KK, KM, KFT

Project administration: MT

Resources: TM, IH

Supervision: MT

Visualization: RKK, SU, MT

Writing–original draft: RKK, SU, KY, MT

Writing–review and editing: RKK, SU, MT

Funding

Funder	Grant reference number	Author
MEXT | Japan Society for the Promotion of Science (JSPS)	JP19H05658	Makoto Tsuda
MEXT | Japan Society for the Promotion of Science (JSPS)	JP20H05900	Makoto Tsuda
MEXT | Japan Society for the Promotion of Science (JSPS)	JP24H00067	Makoto Tsuda
MEXT | Japan Society for the Promotion of Science (JSPS)	JP22KJ2471	Riku Kawanabe-Kobayashi
MEXT | Japan Society for the Promotion of Science (JSPS)	JP23KJ1729	Sawako Uchiyama
MEXT | Japan Society for the Promotion of Science (JSPS)	JP19J21063	Kohei Yoshihara
Japan Agency for Medical Research and Development (AMED)	25gm1510013h	Makoto Tsuda
Japan Agency for Medical Research and Development (AMED)	JP25ama121031	Makoto Tsuda

Author ORCID iDs

Thomas McHugh: https://orcid.org/0000-0002-1243-5189
Kenji F Tanaka: https://orcid.org/0000-0003-2511-0057
Makoto Tsuda: https://orcid.org/0000-0003-0585-9570

Additional files

Figures S1–8

Table S1

Movie

References

1 **Todd A. J** (2010) Neuronal circuitry for pain processing in the dorsal horn. *Nat Rev Neurosci* **11**:823-836 https://doi.org/10.1038/nrn2947

2 **Peirs C.,** Seal R. P (2016) Neural circuits for pain: Recent advances and current views. *Science* **354**:578-584 https://doi.org/10.1126/science.aaf8933

3 **Koch S. C.,** Acton D., Goulding M (2018) Spinal Circuits for Touch, Pain, and Itch. *Annu Rev Physiol* **80**:189-217 https://doi.org/10.1146/annurev-physiol-022516-034303

4 **Moehring F.,** Halder P., Seal R. P., Stucky C. L (2018) Uncovering the Cells and Circuits of Touch in Normal and Pathological Settings. *Neuron* **100**:349-360 https://doi.org/10.1016/j.neuron.2018.10.019

5 **Peirs C.,** Dallel R., Todd A. J (2020) Recent advances in our understanding of the organization of dorsal horn neuron populations and their contribution to cutaneous mechanical allodynia. *J Neural Transm* **127**:505-525 https://doi.org/10.1007/s00702-020-02159-1

6 **Wang L. H.,** Ding W. Q., Sun Y. G (2022) Spinal ascending pathways for somatosensory information processing. *Trends Neurosci* **45**:594-607 https://doi.org/10.1016/j.tins.2022.05.005

7 **Mercer Lindsay N.,** Chen C., Gilam G., Mackey S., Scherrer G. (2021) Brain circuits for pain and its treatment. *Sci Transl Med* **13**:eabj7360 https://doi.org/10.1126/scitranslmed.abj7360

8 **Nguyen E.,** Grajales-Reyes J. G., Gereau R. W. t., Ross S. E. (2023) Cell type-specific dissection of sensory pathways involved in descending modulation. *Trends Neurosci* **46**:539-550 https://doi.org/10.1016/j.tins.2023.04.002

9 **Yoshimura M.,** Furue H (2006) Mechanisms for the anti-nociceptive actions of the descending noradrenergic and serotonergic systems in the spinal cord. *J Pharmacol Sci* **101**:107-117 https://doi.org/10.1254/jphs.crj06008x

10 **Llorca-Torralba M.,** Borges G., Neto F., Mico J. A., Berrocoso E (2016) Noradrenergic Locus Coeruleus pathways in pain modulation. *Neuroscience* **338**:93-113 https://doi.org/10.1016/j.neuroscience.2016.05.057

11 **Suárez-Pereira I.,** et al. (2022) The Role of the Locus Coeruleus in Pain and Associated Stress-Related Disorders. *Biol Psychiatry* **91**:786-797 https://doi.org/10.1016/j.biopsych.2021.11.023

12 **Li J.,** et al. (2022) Activation of locus coeruleus-spinal cord noradrenergic neurons alleviates neuropathic pain in mice via reducing neuroinflammation from astrocytes and microglia in spinal dorsal horn. *J Neuroinflammation* **19**:123 https://doi.org/10.1186/s12974-022-02489-9

13 **Häring M.,** et al. (2018) Neuronal atlas of the dorsal horn defines its architecture and links sensory input to transcriptional cell types. *Nat Neurosci* **21**:869-880 https://doi.org/10.1038/s41593-018-0141-1

14 **Shiraishi Y.,** et al. (2021) α1A-adrenaline receptors in dorsal horn inhibitory neurons have an inhibitory role in the regulation of chloroquine-induced itch in mice. *Mol Brain* **14** https://doi.org/10.1186/s13041-021-00768-9

15 **Baba H.,** et al. (2000) Norepinephrine facilitates inhibitory transmission in substantia gelatinosa of adult rat spinal cord (part 2): effects on somatodendritic sites of GABAergic neurons. *Anesthesiology* **92**:485-492 https://doi.org/10.1097/00000542-200002000-00031

16 **Uchiyama S.,** et al. (2022) Stress-induced antinociception to noxious heat requires α1A-adrenaline receptors of spinal inhibitory neurons in mice. *Mol Brain* **15**:6 https://doi.org/10.1186/s13041-021-00895-3

17 **Inoue K.,** Tsuda M (2018) Microglia in neuropathic pain: cellular and molecular mechanisms and therapeutic potential. *Nat Rev Neurosci* **19**:138-152 https://doi.org/10.1038/nrn.2018.2

18 **Ji R. R.,** Donnelly C. R., Nedergaard M (2019) Astrocytes in chronic pain and itch. *Nat Rev Neurosci* **20**:667-685 https://doi.org/10.1038/s41583-019-0218-1

19 **Tsuda M.,** Masuda T., Kohno K (2023) Microglial diversity in neuropathic pain. *Trends Neurosci* **46**:597-610 https://doi.org/10.1016/j.tins.2023.05.001

20 **Sekiguchi K. J.,** et al. (2016) Imaging large-scale cellular activity in spinal cord of freely behaving mice. *Nat Commun* **7**:11450 https://doi.org/10.1038/ncomms11450

21 **Yoshihara K.,** et al. (2018) Astrocytic Ca(2+) responses in the spinal dorsal horn by noxious stimuli to the skin. *J Pharmacol Sci* **137**:101-104 https://doi.org/10.1016/j.jphs.2018.04.007

22 **Kohro Y.,** et al. (2020) Spinal astrocytes in superficial laminae gate brainstem descending control of mechanosensory hypersensitivity. *Nat Neurosci* **23**:1376-1387 https://doi.org/10.1038/s41593-020-00713-4

23 **Kawanabe R.,** Yoshihara K., Hatada I., Tsuda M (2021) Activation of spinal dorsal horn astrocytes by noxious stimuli involves descending noradrenergic signaling. *Mol Brain* **14**:79 https://doi.org/10.1186/s13041-021-00788-5

24 **Hertz L.,** Lovatt D., Goldman S. A., Nedergaard M (2010) Adrenoceptors in brain: cellular gene expression and effects on astrocytic metabolism and [Ca(2+)]i. *Neurochem Int* **57**:411-420 https://doi.org/10.1016/j.neuint.2010.03.019

25 **Bazargani N.,** Attwell D (2016) Astrocyte calcium signaling: the third wave. *Nat Neurosci* **19**:182-189 https://doi.org/10.1038/nn.4201

26 **Batiuk M. Y.,** et al. (2020) Identification of region-specific astrocyte subtypes at single cell resolution. *Nat Commun* **11**:1220 https://doi.org/10.1038/s41467-019-14198-8

27 **Wahis J.,** et al. (2024) The astrocyte α1A-adrenoreceptor is a key component of the neuromodulatory system in mouse visual cortex. *Glia* https://doi.org/10.1002/glia.24591

28 **Cohen Z.,** Molinatti G., Hamel E (1997) Astroglial and vascular interactions of noradrenaline terminals in the rat cerebral cortex. *J Cereb Blood Flow Metab* **17**:894-904 https://doi.org/10.1097/00004647-199708000-00008

29 **Valentino R. J.,** Van Bockstaele E (2008) Convergent regulation of locus coeruleus activity as an adaptive response to stress. *Eur J Pharmacol* **583**:194-203 https://doi.org/10.1016/j.ejphar.2007.11.062

30 **Imbe H.,** et al. (2009) Activation of ERK in the locus coeruleus following acute noxious stimulation. *Brain Res* **1263**:50-57 https://doi.org/10.1016/j.brainres.2009.01.052

31 **Chen F. J.,** Sara S. J (2007) Locus coeruleus activation by foot shock or electrical stimulation inhibits amygdala neurons. *Neuroscience* **144**:472-481 https://doi.org/10.1016/j.neuroscience.2006.09.037

32 **McCall J. G.,** et al. (2015) CRH Engagement of the Locus Coeruleus Noradrenergic System Mediates Stress-Induced Anxiety. *Neuron* **87**:605-620 https://doi.org/10.1016/j.neuron.2015.07.002

33 **Butler R. K.,** Finn D. P. (2009) Stress-induced analgesia. *Prog Neurobiol* **88**:184-202 https://doi.org/10.1016/j.pneurobio.2009.04.003

34 **Jennings E. M.,** Okine B. N., Roche M., Finn D. P. (2014) Stress-induced hyperalgesia. *Prog Neurobiol* **121**:1-18 https://doi.org/10.1016/j.pneurobio.2014.06.003

35 **François A.,** et al. (2017) A Brainstem-Spinal Cord Inhibitory Circuit for Mechanical Pain Modulation by GABA and Enkephalins. *Neuron* **93**:822-839.e826 https://doi.org/10.1016/j.neuron.2017.01.008

36 **Abdallah C. G.,** Geha P (2017) Chronic Pain and Chronic Stress: Two Sides of the Same Coin?. *Chronic Stress* **1** https://doi.org/10.1177/2470547017704763

37 **Fitzcharles M. A.,** et al. (2021) Nociplastic pain: towards an understanding of prevalent pain conditions. *Lancet* **397**:2098-2110 https://doi.org/10.1016/s0140-6736(21)00392-5

38 **Sousa F. S. S.,** et al. (2018) α-(phenylselanyl) acetophenone abolishes acute restraint stress induced-comorbid pain, depression and anxiety-related behaviors in mice. *Neurochem Int* **120**:112-120 https://doi.org/10.1016/j.neuint.2018.08.006

39 **Contet C.,** et al. (2006) Dissociation of analgesic and hormonal responses to forced swim stress using opioid receptor knockout mice. *Neuropsychopharmacology* **31**:1733-1744 https://doi.org/10.1038/sj.npp.1300934

40 **Kim J. W.,** et al. (2018) Social support rescues acute stress-induced cognitive impairments by modulating ERK1/2 phosphorylation in adolescent mice. *Sci Rep* **8**:12003 https://doi.org/10.1038/s41598-018-30524-4

41 **Wagatsuma A.,** et al. (2018) Locus coeruleus input to hippocampal CA3 drives single-trial learning of a novel context. *Proc Natl Acad Sci U S A* **115**:E310-E316 https://doi.org/10.1073/pnas.1714082115

42 **Mulvey B.,** et al. (2018) Molecular and Functional Sex Differences of Noradrenergic Neurons in the Mouse Locus Coeruleus. *Cell Rep* **23**:2225-2235 https://doi.org/10.1016/j.celrep.2018.04.054

43 **Saito M.,** et al. (2001) Diphtheria toxin receptor-mediated conditional and targeted cell ablation in transgenic mice. *Nat Biotechnol* **19**:746-750 https://doi.org/10.1038/90795

44 **Klapoetke N. C.,** et al. (2014) Independent optical excitation of distinct neural populations. *Nat Methods* **11**:338-346 https://doi.org/10.1038/nmeth.2836

45 **Feng J.,** et al. (2019) A Genetically Encoded Fluorescent Sensor for Rapid and Specific In Vivo Detection of Norepinephrine. *Neuron* **102**:745-761.e748, https://doi.org/10.1016/j.neuron.2019.02.037

46 **Lee Y.,** Messing A., Su M., Brenner M (2008) GFAP promoter elements required for region-specific and astrocyte-specific expression. *Glia* **56**:481-493 https://doi.org/10.1002/glia.20622

47 **Nam Y.,** et al. (2016) Reversible Induction of Pain Hypersensitivity following Optogenetic Stimulation of Spinal Astrocytes. *Cell Rep* **17**:3049-3061 https://doi.org/10.1016/j.celrep.2016.11.043

48 **Wu S. H.,** Ma C. L., Kelly J. B. (2004) Contribution of AMPA, NMDA, and GABA(A) receptors to temporal pattern of postsynaptic responses in the inferior colliculus of the rat. *J Neurosci* **24**:4625-4634 https://doi.org/10.1523/JNEUROSCI.0318-04.2004

49 **Liu J.,** Wu D. C., Wang Y. T (2010) Allosteric potentiation of glycine receptor chloride currents by glutamate. *Nat Neurosci* **13**:1225-1232 https://doi.org/10.1038/nn.2633

50 **Metzner K.,** et al. (2021) Lack of efficacy of a partial adenosine A1 receptor agonist in neuropathic pain models in mice. *Purinergic Signal* **17**:503-514 https://doi.org/10.1007/s11302-021-09806-6

51 **Cui X.,** et al. (2024) Enhancing spinal cord stimulation-induced pain inhibition by augmenting endogenous adenosine signalling after nerve injury in rats. *Br J Anaesth* **132**:746-757 https://doi.org/10.1016/j.bja.2024.01.005

52 **Ran F. A.,** et al. (2015) In vivo genome editing using Staphylococcus aureus Cas9. *Nature* **520**:186-191 https://doi.org/10.1038/nature14299

53 **Cheng L.,** et al. (2004) Tlx3 and Tlx1 are post-mitotic selector genes determining glutamatergic over GABAergic cell fates. *Nat Neurosci* **7**:510-517 https://doi.org/10.1038/nn1221

54 **Roth B. L.** (2016) DREADDs for Neuroscientists. *Neuron* **89**:683-694 https://doi.org/10.1016/j.neuron.2016.01.040

55 **Kagiyama I.,** Uchiyama S., Tsuda M (2025) Hes5(+) astrocytes potentiate primary afferent Adelta and C fiber-mediated excitatory synaptic transmission to spinal lamina I neurons. *Mol Brain* **18**:39 https://doi.org/10.1186/s13041-025-01212-y

56 **Ji R. R.,** Baba H., Brenner G. J., Woolf C. J (1999) Nociceptive-specific activation of ERK in spinal neurons contributes to pain hypersensitivity. *Nat Neurosci* **2**:1114-1119 https://doi.org/10.1038/16040

57 **Matsumoto M.,** Xie W., Ma L., Ueda H (2008) Pharmacological switch in Abeta-fiber stimulation-induced spinal transmission in mice with partial sciatic nerve injury. *Mol Pain* **4**:25 https://doi.org/10.1186/1744-8069-4-25

58 **Kawabata R.,** et al. (2023) The Anterior Cingulate Cortex is Critical for Acute Stress-induced Hypersensitivity in Mice. *Neuroscience* **523**:47-60 https://doi.org/10.1016/j.neuroscience.2023.05.010

59 **Hickey L.,** et al. (2014) Optoactivation of locus ceruleus neurons evokes bidirectional changes in thermal nociception in rats. *J Neurosci* **34**:4148-4160 https://doi.org/10.1523/jneurosci.4835-13.2014

60 **Hirschberg S.,** Li Y., Randall A., Kremer E. J., Pickering A. E (2017) Functional dichotomy in spinal-vs prefrontal-projecting locus coeruleus modules splits descending noradrenergic analgesia from ascending aversion and anxiety in rats. *eLife* **6**:e29808 https://doi.org/10.7554/eLife.29808

61 **Duan B.,** et al. (2014) Identification of spinal circuits transmitting and gating mechanical pain. *Cell* **159**:1417-1432 https://doi.org/10.1016/j.cell.2014.11.003

62 **Petitjean H.,** et al. (2015) Dorsal Horn Parvalbumin Neurons Are Gate-Keepers of Touch-Evoked Pain after Nerve Injury. *Cell Rep* **13**:1246-1257 https://doi.org/10.1016/j.celrep.2015.09.080

63 **Wang H.,** et al. (2022) A novel spinal neuron connection for heat sensation. *Neuron* **110**:2315-2333.e2316 https://doi.org/10.1016/j.neuron.2022.04.021

64 **Warwick C.,** et al. (2022) Cell type-specific calcium imaging of central sensitization in mouse dorsal horn. *Nat Commun* **13**:5199 https://doi.org/10.1038/s41467-022-32608-2

65 **Kucharczyk M. W.,** Di Domenico F., Bannister K (2022) Distinct brainstem to spinal cord noradrenergic pathways inversely regulate spinal neuronal activity. *Brain* **145**:2293-2300 https://doi.org/10.1093/brain/awac085

66 **Torsney C.,** MacDermott A. B (2006) Disinhibition opens the gate to pathological pain signaling in superficial neurokinin 1 receptor-expressing neurons in rat spinal cord. *J Neurosci* **26**:1833-1843 https://doi.org/10.1523/jneurosci.4584-05.2006

67 **Sonohata M.,** et al. (2019) Noradrenaline modulates mechanically evoked responses in the rat spinal dorsal horn: an in vivo patch-clamp study. *J Pain Res* **12**:1269-1278 https://doi.org/10.2147/jpr.s181210

68 **Usoskin D.,** et al. (2015) Unbiased classification of sensory neuron types by large-scale single-cell RNA sequencing. *Nat Neurosci* **18**:145-153 https://doi.org/10.1038/nn.3881

69 **Kawasaki Y.,** Kumamoto E., Furue H., Yoshimura M (2003) Alpha 2 adrenoceptor-mediated presynaptic inhibition of primary afferent glutamatergic transmission in rat substantia gelatinosa neurons. *Anesthesiology* **98**:682-689 https://doi.org/10.1097/00000542-200303000-00016

70 **Li X.,** Eisenach J. C (2001) alpha2A-adrenoceptor stimulation reduces capsaicin-induced glutamate release from spinal cord synaptosomes. *J Pharmacol Exp Ther* **299**:939-944

71 **Pankratov Y.,** Lalo U (2015) Role for astroglial α1-adrenoreceptors in gliotransmission and control of synaptic plasticity in the neocortex. *Front Cell Neurosci* **9**:230 https://doi.org/10.3389/fncel.2015.00230

72 **Xu Q.,** et al. (2021) Astrocytes contribute to pain gating in the spinal cord. *Sci Adv* **7**:eabi6287 https://doi.org/10.1126/sciadv.abi6287

73 **Oe Y.,** et al. (2020) Distinct temporal integration of noradrenaline signaling by astrocytic second messengers during vigilance. *Nat Commun* **11**:471 https://doi.org/10.1038/s41467-020-14378-x

74 **Lerman S. F.,** Rudich Z., Brill S., Shalev H., Shahar G (2015) Longitudinal associations between depression, anxiety, pain, and pain-related disability in chronic pain patients. *Psychosom Med* **77**:333-341 https://doi.org/10.1097/psy.0000000000000158

75 **Lugert S.,** et al. (2012) Homeostatic neurogenesis in the adult hippocampus does not involve amplification of Ascl1(high) intermediate progenitors. *Nat Commun* **3**:670 https://doi.org/10.1038/ncomms1670

76 **Vong L.,** et al. (2011) Leptin action on GABAergic neurons prevents obesity and reduces inhibitory tone to POMC neurons. *Neuron* **71**:142-154 https://doi.org/10.1016/j.neuron.2011.05.028

77 **Madisen L.,** et al. (2010) A robust and high-throughput Cre reporting and characterization system for the whole mouse brain. *Nat Neurosci* **13**:133-140 https://doi.org/10.1038/nn.2467

78 **Chaplan S. R.,** Bach F. W., Pogrel J. W., Chung J. M., Yaksh T. L (1994) Quantitative assessment of tactile allodynia in the rat paw. *J Neurosci Methods* **53**:55-63 https://doi.org/10.1016/0165-0270(94)90144-9

79 **Atwal N.,** Winters B. L., Vaughan C. W (2020) Endogenous cannabinoid modulation of restraint stress-induced analgesia in thermal nociception. *J Neurochem* **152**:92-102 https://doi.org/10.1111/jnc.14884

80 **Tsuda M.,** et al. (2009) Behavioral phenotypes of mice lacking purinergic P2X4 receptors in acute and chronic pain assays. *Mol Pain* **5**:28 https://doi.org/10.1186/1744-8069-5-28

81 **Kohro Y.,** et al. (2015) A new minimally-invasive method for microinjection into the mouse spinal dorsal horn. *Sci Rep* **5**:14306 https://doi.org/10.1038/srep14306

82 **Zhang Z. M.,** Chen S., Liang Y. Z (2010) Baseline correction using adaptive iteratively reweighted penalized least squares. *Analyst* **135**:1138-1146 https://doi.org/10.1039/b922045c

83 **Thévenaz P.,** Ruttimann U. E., Unser M (1998) A pyramid approach to subpixel registration based on intensity. *IEEE Trans Image Process* **7**:27-41 https://doi.org/10.1109/83.650848

Peer reviews

Reviewer #1 (Public review):

Review of the revised submission:

I thank the authors for their detailed consideration of my comments and for the additional data, analyses, and clarifications they have incorporated. The new behavioral experiments, quantification of targeted manipulations, and expanded methodological details strengthen the manuscript and address many of my initial concerns. While some questions remain for future work, the authors' careful responses and the additional evidence provided help resolve the main issues I raised, and I am generally satisfied with the revisions.

Review of original submission:

Summary

In this article, Kawanabe-Kobayashi et al., aim to examine the mechanisms by which stress can modulate pain in mice. They focus on the contribution of noradrenergic neurons (NA) of the locus coeruleus (LC). The authors use acute restraint stress as a stress paradigm and found that following one hour of restraint stress mice display mechanical hypersensitivity. They show that restraint stress causes the activation of LC NA neurons and the release of NA in the spinal cord dorsal horn (SDH). They then examine the spinal mechanisms by which LC→SDH NA produces mechanical hypersensitivity. The authors provide evidence that NA can act on alphaA1Rs expressed by a class of astrocytes defined by the expression of Hes (Hes+). Furthermore, they found that NA, presumably through astrocytic release of ATP following NA action on alphaA1Rs Hes+ astrocytes, can cause an adenosine-mediated inhibition of SDH inhibitory interneurons. They propose that this disinhibition mechanism could explain how restraint stress can cause the mechanical hypersensitivity they measured in their behavioral experiments.

Strengths:

(1) Significance. Stress profoundly influences pain perception; resolving the mechanisms by which stress alters nociception in rodents may explain the well-known phenomenon of stress-induced analgesia and/or facilitate the development of therapies to mitigate the negative consequences of chronic stress on chronic pain.

(2) Novelty. The authors' findings reveal a crucial contribution of Hes+ spinal astrocytes in the modulation of pain thresholds during stress.

(3) Techniques. This study combines multiple approaches to dissect circuit, cellular, and molecular mechanisms including optical recordings of neural and astrocytic Ca2+ activity in behaving mice, intersectional genetic strategies, cell ablation, optogenetics, chemogenetics, CRISPR-based gene knockdown, slice electrophysiology, and behavior.

Weaknesses:

(1) Mouse model of stress. Although chronic stress can increase sensitivity to somatosensory stimuli and contribute to hyperalgesia and anhedonia, particularly in the context of chronic pain states, acute stress is well known to produce analgesia in humans and rodents. The experimental design used by the authors consists of a single one-hour session of restraint stress followed by 30 min to one hour of habituation and measurement of cutaneous mechanical sensitivity with von Frey filaments. This acute stress behavioral paradigm corresponds to the conditions in which the clinical phenomenon of stress-induced analgesia is observed in humans, as well as in animal models. Surprisingly, however, the authors

measured that this acute stressor produced hypersensitivity rather than antinociception. This discrepancy is significant and requires further investigation.

(2) Specifically, is the hypersensitivity to mechanical stimulation also observed in response to heat or cold on a hotplate or coldplate?

(3) Using other stress models, such as a forced swim, do the authors also observe acute stress-induced hypersensitivity instead of stress-induced antinociception?

(4) Measurement of stress hormones in blood would provide an objective measure of the stress of the animals.

(5) Results:

(a) Optical recordings of Ca2+ activity in behaving rodents are particularly useful to investigate the relationship between Ca2+ dynamics and the behaviors displayed by rodents.

(b) The authors report an increase in Ca2+ events in LC NA neurons during restraint stress: Did mice display specific behaviors at the time these Ca2+ events were observed such as movements to escape or orofacial behaviors including head movements or whisking?

(c) Additionally, are similar increases in Ca2+ events in LC NA neurons observed during other stressful behavioral paradigms versus non-stressful paradigms?

(d) Neuronal ablation to reveal the function of a cell population.

(e) The proportion of LC NA neurons and LC→SDH NA neurons expressing DTR-GFP and ablated should be quantified (Figures 1G and J) to validate the methods and permit interpretation of the behavioral data (Figures 1H and K). Importantly, the nocifensive responses and behavior of these mice in other pain assays in the absence of stress (e.g., hotplate) and a few standard assays (open field, rotarod, elevated plus maze) would help determine the consequences of cell ablation on processing of nociceptive information and general behavior.

(f) Confirmation of LC NA neuron function with other methods that alter neuronal excitability or neurotransmission instead of destroying the circuit investigated, such as chemogenetics or chemogenetics, would greatly strengthen the findings. Optogenetics is used in Figure 1M, N but excitation of LC→SDH NA neuron terminals is tested instead of inhibition (to mimic ablation), and in naïve mice instead of stressed mice.

(g) Alpha1Ars. The authors noted that "Adra1a mRNA is also expressed in INs in the SDH".

(h) The authors should comprehensively indicate what other cell types present in the spinal cord and neurons projecting to the spinal cord express alpha1Ars and what is the relative expression level of alpha1Ars in these different cell types.

(i) The conditional KO of alpha1Ars specifically in Hes5+ astrocytes and not in other cell types expressing alpha1Ars should be quantified and validated (Figure 2H).

(j) Depolarization of SDH inhibitory interneurons by NA (Figure 3). The authors' bath applied NA, which presumably activates all NA receptors present in the preparation.

k) The authors' model (Figure 4H) implies that NA released by LC→SDH NA neurons leads to the inhibition of SDH inhibitory interneurons by NA. In other experiments (Figure 1L, Figure 2A), the authors used optogenetics to promote the release of endogenous NA in SDH by LC→SDH NA neurons. This approach would investigate the function of NA endogenously released by LC NA neurons at presynaptic terminals in the SDH and at physiological concentrations and would test the model more convincingly compared to the bath application of NA.

(l) As for other experiments, the proportion of Hes+ astrocytes that express hM3Dq, and the absence of expression in other cells, should be quantified and validated to interpret behavioral data.

(m) Showing that the effect of CNO is dose-dependent would strengthen the authors' findings.

(n) The proportion of SG neurons for which CNO bath application resulted in a reduction in recorded sIPSCs is not clear.

(o) A1Rs. The specific expression of Cas9 and guide RNAs, and the specific KD of A1Rs, in inhibitory interneurons but not in other cell types expressing A1Rs should be quantified and validated.

(6) Methods:

It is unclear how fiber photometry is performed using "optic cannula" during restraint stress while mice are in a 50ml falcon tube (as shown in Figure 1A).

https://doi.org/10.7554/eLife.104453.2.sa3

Reviewer #2 (Public review):

Summary:

This study investigates the role of spinal astrocytes in mediating stress-induced pain hypersensitivity, focusing on the LC (locus coeruleus)-to-SDH (spinal dorsal horn) circuit and its mechanisms. The authors aimed to delineate how LC activity contributes to spinal astrocytic activation under stress conditions, explore the role of noradrenaline (NA) signaling in this process, and identify the downstream astrocytic mechanisms that influence pain hypersensitivity.

The authors provide strong evidence that 1-hour restraint stress-induced pain hypersensitivity involves the LC-to-SDH circuit, where NA triggers astrocytic calcium activity via alpha1a adrenoceptors (alpha1aRs). Blockade of alpha1aRs on astrocytes-but not on Vgat-positive SDH neurons-reduced stress-induced pain hypersensitivity. These findings are rigorously supported by well-established behavioral models and advanced genetic techniques, uncovering the critical role of spinal astrocytes in modulating stress-induced pain.

However, the study's third aim-to establish a pathway from astrocyte alpha1aRs to adenosine-mediated inhibition of SDH-Vgat neurons-is less compelling. While pharmacological and behavioral evidence is intriguing, the ex vivo findings are indirect and lack a clear connection to the stress-induced pain model. Despite these limitations, the study advances our understanding of astrocyte-neuron interactions in stress-pain contexts and provides a strong foundation for future research into glial mechanisms in pain hypersensitivity.

Strengths:

The study is built on a robust experimental design using a validated 1-hour restraint stress model, providing a reliable framework to investigate stress-induced pain hypersensitivity. The authors utilized advanced genetic tools, including retrograde AAVs, optogenetics, chemogenetics, and subpopulation-specific knockouts, allowing precise manipulation and interrogation of the LC-SDH circuit and astrocytic roles in pain modulation. Clear evidence demonstrates that NA triggers astrocytic calcium activity via alpha1aRs, and blocking these receptors effectively reduces stress-induced pain hypersensitivity.

Weaknesses:

The study offers mainly indirect evidence for astrocyte-released adenosine acting on SDH-VGAT neurons. The potential contributions of astrocyte-derived D-serine and adenosine to different spinal neuron subtypes, as well as the transient "dip" in astrocytic calcium following LC optostimulation, merit further clarification in future work once appropriate tools become available.

Comments on revisions:

The authors have thoroughly addressed my previous comments, resolving most of the points I raised except those noted in the "Weaknesses" section above. I understand that some of these aspects will require future tool development.

https://doi.org/10.7554/eLife.104453.2.sa2

Reviewer #3 (Public review):

Summary

This is an exciting and timely study addressing the role of descending noradrenergic systems in nocifensive responses. While it is well-established that spinally released noradrenaline (aka norepinephrine) generally acts as an inhibitory factor in spinal sensory processing, this system is highly complex. Descending projections from the A6 (locus coeruleus, LC) and the A5 regions typically modulate spinal sensory processing and reduce pain behaviours, but certain subpopulations of LC neurons have been shown to mediate pronociceptive effects, such as those projecting to the prefrontal cortex (Hirshberg et al., PMID: 29027903).

The study proposes that descending cerulean noradrenergic neurons potentiate touch sensation via alpha-1 adrenoceptors on Hes5+ spinal astrocytes, contributing to mechanical hyperalgesia. This finding is consistent with prior work from the same group (dd et al., PMID:). However, caution is needed when generalising about LC projections, as the locus coeruleus is functionally diverse, with differences in targets, neurotransmitter co-release, and behavioural effects. Specifying the subpopulations of LC neurons involved would significantly enhance the impact and interpretability of the findings.

Strengths

The study employs state-of-the-art molecular, genetic, and neurophysiological methods, including precise CRISPR and optogenetic targeting, to investigate the role of Hes5+ astrocytes. This approach is elegant and highlights the often-overlooked contribution of astrocytes in spinal sensory gating. The data convincingly support the role of Hes5+ astrocytes as regulators of touch sensation, coordinated by brain-derived noradrenaline in the spinal dorsal horn, opening new avenues for research into pain and touch modulation.

Furthermore, the data support a model in which superficial dorsal horn (SDH) Hes5+ astrocytes act as non-neuronal gating cells for brain-derived noradrenergic (NA) signalling through their interaction with substantia gelatinosa inhibitory interneurons. Locally released adenosine from NA-stimulated Hes5+ astrocytes, following acute restraint stress, may suppress the function of SDH-Vgat+ inhibitory interneurons, resulting in mechanical pain hypersensitivity. However, the spatially restricted neuron-astrocyte communication underlying this mechanism requires further investigation in future studies.

Comments on revisions:

One important point remains insufficiently resolved. In Figure S4C, two of the three visible neurons in the A5 example appear to show a white "halo" at the cell border, suggesting a

merge of eGFP (green) and TH (magenta) and therefore possible transgene positivity. To draw a confident conclusion about the specificity of the approach for the A6 (LC) population, the authors are kindly asked to provide high-resolution images of several representative A5 sections, presented both as merged and as separate colour channels. Ideally, quantification across multiple rostrocaudal sections of A5, A6 and A7 should be provided. This is essential for determining whether any transgene expression occurs within the A5 nucleus, particularly given its several-millimetre rostrocaudal extent. As the behavioural phenotype arises from manipulation of only a small subset of A6 neurons, ruling out any contribution from A5 (or A7) is critical for validating pathway specificity, especially in light of prior reports showing that similar approaches can label A5 fibres.

https://doi.org/10.7554/eLife.104453.2.sa1

Author response:

The following is the authors' response to the original reviews.

> ***Public reviews:***
>
> ***Reviewer #1 (Public review):***
>
> *Summary:*
>
> *In this article, Kawanabe-Kobayashi et al., aim to examine the mechanisms by which stress can modulate pain in mice. They focus on the contribution of noradrenergic neurons (NA) of the locus coeruleus (LC). The authors use acute restraint stress as a stress paradigm and found that following one hour of restraint stress mice display mechanical hypersensitivity. They show that restraint stress causes the activation of LC NA neurons and the release of NA in the spinal cord dorsal horn (SDH). They then examine the spinal mechanisms by which LC→SDH NA produces mechanical hypersensitivity. The authors provide evidence that NA can act on alphaA1Rs expressed by a class of astrocytes defined by the expression of Hes (Hes+). Furthermore, they found that NA, presumably through astrocytic release of ATP following NA action on alphaA1Rs Hes+ astrocytes, can cause an adenosine-mediated inhibition of SDH inhibitory interneurons. They propose that this disinhibition mechanism could explain how restraint stress can cause the mechanical hypersensitivity they measured in their behavioral experiments.*
>
> *Strengths:*
>
> *(1) Significance. Stress profoundly influences pain perception; resolving the mechanisms by which stress alters nociception in rodents may explain the well-known phenomenon of stress-induced analgesia and/or facilitate the development of therapies to mitigate the negative consequences of chronic stress on chronic pain.*
>
> *(2) Novelty. The authors' findings reveal a crucial contribution of Hes+ spinal astrocytes in the modulation of pain thresholds during stress.*
>
> *(3) Techniques. This study combines multiple approaches to dissect circuit, cellular, and molecular mechanisms including optical recordings of neural and astrocytic Ca2+ activity in behaving mice, intersectional genetic strategies, cell ablation, optogenetics, chemogenetics, CRISPR-based gene knockdown, slice electrophysiology, and behavior.*
>
> *Weaknesses:*
>
> *(1) Mouse model of stress. Although chronic stress can increase sensitivity to somatosensory stimuli and contribute to hyperalgesia and anhedonia, particularly in the context of chronic pain states, acute stress is well known to produce analgesia in humans*

> *and rodents. The experimental design used by the authors consists of a single one-hour session of restraint stress followed by 30 min to one hour of habituation and measurement of cutaneous mechanical sensitivity with von Frey filaments. This acute stress behavioral paradigm corresponds to the conditions in which the clinical phenomenon of stress-induced analgesia is observed in humans, as well as in animal models. Surprisingly, however, the authors measured that this acute stressor produced hypersensitivity rather than antinociception. This discrepancy is significant and requires further investigation.*

We thank the reviewer for evaluating our work and for highlighting both its strengths and weaknesses. As stated by the reviewer, numerous studies have reported acute stress-induced antinociception. However, as shown in a new additional table (Table S1) in which we have summarized previously published data using the acute restraint stress model employed in our present study, most studies reporting antinociceptive effects of acute restraint stress assessed behavioral responses to heat stimuli or formalin. This observation is consistent with the findings from our previous study (Uchiyama et al., Mol Brain, 2022 (PMID: 34980215)). The present study also confirms that acute restraint stress reduces behavioral responses to noxious heat (see also our response to Comment #2 below). In contrast to the robust and consistent antinociceptive effects observed with thermal stimuli, some studies evaluating behavioral responses to mechanical stimuli have reported stress-induced hypersensitivity (see Table S1), which aligns with our current findings. Taken together, these data support our original notion that the effects of acute stress on pain-related behaviors depend on several factors, including the nature, duration, and intensity of the stressor, as well as the sensory modality assessed in behavioral tests. We have incorporated this discussion and Table S1 into the revised manuscript (lines 344-353). Furthermore, we have slightly modified the text including the title, replacing "pain facilitation" with "mechanical pain hypersensitivity" to more accurately reflect our research focus and the conclusion of this study that $LC^{\rightarrow SDH}$ NAergic signaling to spinal astrocytes is required for stress-induced mechanical pain hypersensitivity. Finally, while mouse models of stress could provide valuable insights, the clinical relevance of stress-induced mechanical pain hypersensitivity remains to be elucidated and requires further investigation. We hope these clarifications address your concerns.

> *(2) Specifically, is the hypersensitivity to mechanical stimulation also observed in response to heat or cold on a hotplate or coldplate?*

Thank you for your important comment. We have now conducted additional behavioral experiments to assess responses to heat using the hot-plate test. We found that mice subjected to restraint stress did not exhibit behavioral hypersensitivity to heat stimuli; instead, they displayed antinociceptive responses (Figure S2; lines 95-98). These results are consistent with our previous findings (Uchiyama et al., Mol Brain, 2022 (PMID: 34980215)) as well as numerous other reports (Table S1).

> *(3) Using other stress models, such as a forced swim, do the authors also observe acute stress-induced hypersensitivity instead of stress-induced antinociception?*

As suggested by the reviewer, we conducted a forced swim test. We found that mice subjected to forced swimming, which has been reported to produce analgesic effects on thermal stimuli (Contet et al., Neuropsychopharmacology, 2006 (PMID: 16237385)), did not exhibit any changes in mechanical pain hypersensitivity (Figure S2; lines 98-99). Furthermore, a previous study demonstrated that mechanical pain sensitivity is enhanced by other stress models, such as exposure to an elevated open platform for 30 min (Kawabata et al., Neuroscience, 2023 (PMID: 37211084)). However, considering our data showing that changes in mechanosensory behavior induced by restraint stress depend on the duration of exposure (Figure S1), and that restraint stress also produced an antinociceptive effect on heat stimuli (Figure S2), stress-induced modulation of pain is a complex phenomenon influenced by multiple factors,

including the stress model, intensity, and duration, as well as the sensory modality used for behavioral testing (lines 100-103).

> *(4) Measurement of stress hormones in blood would provide an objective measure of the stress of the animals.*

A previous study has demonstrated that plasma corticosterone levels—a stress hormone—are elevated following a 1-hour exposure to restraint stress in mice (Kim et al., Sci Rep, 2018 (PMID: 30104581)), using a stress protocol similar to that employed in our current study. We have included this information with citing this paper (lines 104-105).

> *(5) Results:*
>
> *(a) Optical recordings of Ca2+ activity in behaving rodents are particularly useful to investigate the relationship between Ca2+ dynamics and the behaviors displayed by rodents.*

In the optical recordings of Ca^{2+} activity in LC neurons, we monitored mouse behavior during stress exposure. We have now included a video of this in the revised manuscript (video; lines 111-114).

> *(b) The authors report an increase in Ca2+ events in LC NA neurons during restraint stress: Did mice display specific behaviors at the time these Ca2+ events were observed such as movements to escape or orofacial behaviors including head movements or whisking?*

By reanalyzing the temporal relationship between Ca^{2+} events and mouse behavior during stress exposure, we found that the Ca^{2+} transients and escape behaviors (struggling) occurred almost simultaneously (video). A similar temporal correlation is also observed in Ca^{2+} responses in the bed nucleus of the stria terminalis (Luchsinger et al., Nat Commun, 2021 (PMID: 34117229)). The video file has been included in the revised manuscript (video; lines 111-113, 552-553, 573-575).

Additionally, as described in the Methods section and shown in Figure S2 of the initial version (now Figure S3), non-specific signals or artifacts—such as those caused by head movements—were corrected (although such responses were minimal in our recordings).

> *(c) Additionally, are similar increases in Ca2+ events in LC NA neurons observed during other stressful behavioral paradigms versus non-stressful paradigms?*

We appreciate the reviewer's valuable suggestion. Since the present, initial version of our manuscript focused on acute restraint stress, we did not measure Ca^{2+} events in LC-NA neurons in other stress models, but a recent study has shown an increase in Ca^{2+} responses in LC-NA neurons by social defeat stress (Seiriki et al., BioRxiv, *https://www.biorxiv.org/content/10.1101/2025.03.07.641347v1*).

> *(d) Neuronal ablation to reveal the function of a cell population.*

This method has been widely used in numerous previous studies as an effective experimental approach to investigate the role of specific neuronal populations—including SDH-projecting LC-NA neurons (Ma et al., Brain Res, 2022 (PMID: 34929182); Kawanabe et al., Mol Brain, 2021 (PMID: 33971918))—in CNS function.

> *(e) The proportion of LC NA neurons and LC→SDH NA neurons expressing DTR-GFP and ablated should be quantified (Figures 1G and J) to validate the methods and permit interpretation of the behavioral data (Figures 1H and K). Importantly, the nocifensive responses and behavior of these mice in other pain assays in the absence of stress (e.g., hotplate) and a few standard assays (open field, rotarod, elevated plus maze) would help*

> *determine the consequences of cell ablation on processing of nociceptive information and general behavior.*

As suggested, we conducted additional experiments to quantitatively analyze the number of $LC^{\rightarrow SDH}$-NA neurons. We used WT mice injected with AAVretro-Cre into the SDH (L4 segment) and AAV-FLEx[DTR-EGFP] into the LC. In these mice, 4.4% of total LC-NA neurons [positive for tyrosine hydroxylase (TH)] expressed DTR-GFP, representing the $LC^{\rightarrow SDH}$-NA neuronal population (Figure S4; lines 126-127). Furthermore, treatment with DTX successfully ablated the DTR-expressing $LC^{\rightarrow SDH}$-NA neurons. Importantly, the neurons quantified in this analysis were specifically those projecting to the L4 segment of the SDH; therefore, the total number of SDH-projecting LC-NA neurons across all spinal segments is expected to be much higher.

We also performed the rotarod and paw-flick tests to assess motor function and thermal sensitivity following ablation of $LC^{\rightarrow SDH}$-NA neurons. No significant differences were observed between the ablated and control groups (Figure S5; lines 131-134), indicating that ablation of these neurons does not produce non-specific behavioral deficits in motor function or other sensory modalities.

> *(f) Confirmation of LC NA neuron function with other methods that alter neuronal excitability or neurotransmission instead of destroying the circuit investigated, such as chemogenetics or chemogenetics, would greatly strengthen the findings. Optogenetics is used in Figure 1M, N but excitation of $LCLC^{\rightarrow SDH}$ NA neuron terminals is tested instead of inhibition (to mimic ablation), and in naïve mice instead of stressed mice.*

We appreciate the reviewer's comment. The optogenetic approach is useful for manipulating neuronal excitability; however, prolonged light illumination (> tens of seconds) can lead to undesirable tissue heating, ionic imbalance, and rebound spikes (Wiegert et al., Neuron, 2017 (PMID: 28772120)), making it difficult to apply in our experiments, in which mice are exposed to stress for 60 min. For this reason, we decided to employ the cell-ablation approach in stress experiments, as it is more suitable than optogenetic inhibition. In addition, as described in our response to weakness (1)-a) by Reviewer 3 (Public review), we have now demonstrated the specific expression of DTRs in NA neurons in the LC, but not in A5 or A7 (Figure S4; lines 127-128), confirming the specificity of $LCLC^{\rightarrow SDH}$-NAergic pathway targeting in our study. Chemogenetics represent another promising approach to further strengthen our findings on the role of $LCLC^{\rightarrow SDH}$-NA neurons, but this will be an important subject for future studies, as it will require extensive experiments to assess, for example, the effectiveness of chemogenetic inhibition of these neurons during 60 min of restraint stress, as well as optimization of key parameters (e.g., systemic DCZ doses).

> *(g) Alpha1Ars. The authors noted that "Adra1a mRNA is also expressed in INs in the SDH".*

The expression of α_{1A}Rs in inhibitory interneurons in the SDH is consistent with our previous findings (Uchiyama et al., Mol Brain, 2022 (PMID: 34980215)) as well as with scRNA-seq data (*http://linnarssonlab.org/dorsalhorn/*, Häring et al., Nat Neurosci, 2018 (PMID: 29686262)).

> *(h) The authors should comprehensively indicate what other cell types present in the spinal cord and neurons projecting to the spinal cord express alpha1Ars and what is the relative expression level of alpha1Ars in these different cell types.*

According to the scRNA-seq data (*https://seqseek.ninds.nih.gov/genes*, Russ et al., Nat Commun, 2021 (PMID: 34588430); *http://linnarssonlab.org/dorsalhorn/*, Häring et al., Nat Neurosci, 2018 (PMID: 29686262)), we confirmed that α_{1A}Rs are predominantly expressed in astrocytes and inhibitory interneurons in the spinal cord. Also, an α_{1A}R-expressing excitatory neuron population (Glut14) expresses *Tacr1*, *GPR83*, and *Tac1* mRNAs, markers that are known to be enriched in projection neurons of the SDH. This raises the possibility that α_{1A} Rs may also be expressed in a subset of projection neurons, although further experiments are required to confirm this. In DRG neurons, α_{1A}R expression was detected to some extent, but

its level seems to be much lower than in the spinal cord (*http://linnarssonlab.org/drg/* Usoskin et al., Nat Neurosci, 2015 (PMID: 25420068)). Consistent with this, primary afferent glutamatergic synaptic transmission has been shown to be unaffected by α_{1A}R agonists (Kawasaki et al., Anesthesiology, 2003 (PMID: 12606912); Li and Eisenach, JPET, 2001 (PMID: 11714880)). This information has been incorporated into the Discussion section (lines 317-319).

> *(i) The conditional KO of alpha1Ars specifically in Hes5+ astrocytes and not in other cell types expressing alpha1Ars should be quantified and validated (Figure 2H).*

We have previously shown a selective KO of α_{1A}R in Hes5$^+$ astrocytes in the same mouse line (Kohro et al., Nat Neurosci, 2020 (PMID: 33020652)). This information has been included in the revised text (line 166-167).

> *(j) Depolarization of SDH inhibitory interneurons by NA (Figure 3). The authors' bath applied NA, which presumably activates all NA receptors present in the preparation.*

We believe that the reviewer's concern may pertain to the possibility that NA acts on non-Vgat$^+$ neurons, thereby indirectly causing depolarization of Vgat$^+$ neurons. As described in the Method section of the initial version, in our electrophysiological experiments, we added four antagonists for excitatory and inhibitory neurotransmitter receptors—CNQX (AMPA receptor), MK-801 (NMDA receptor), bicuculline ($GABA_A$ receptor), and strychnine (glycine receptor)—to the artificial cerebrospinal fluid to block synaptic inputs from other neurons to the recorded Vgat$^+$ neurons. Since this method is widely used for this purpose in many previous studies (Wu et al., J Neurosci, 2004 (PMID: 15140934); Liu et al., Nat Neurosci, 2010 (PMID: 20835251)), it is reasonable to conclude that NA directly acts on the recorded SDH Vgat$^+$ interneurons to produce excitation (lines 193-196).

> *(k) The authors' model (Figure 4H) implies that NA released by LC→SDH NA neurons leads to the inhibition of SDH inhibitory interneurons by NA. In other experiments (Figure 1L, Figure 2A), the authors used optogenetics to promote the release of endogenous NA in SDH by LC→SDH NA neurons. This approach would investigate the function of NA endogenously released by LC NA neurons at presynaptic terminals in the SDH and at physiological concentrations and would test the model more convincingly compared to the bath application of NA.*

We appreciate the reviewer's valuable comment. As noted, optogenetic stimulation of LC$^{\rightarrow SDH}$-NA neurons would indeed be useful to test this model. However, in our case, it is technically difficult to investigate the responses of Vgat$^+$ inhibitory neurons and Hes5$^+$ astrocytes to NA endogenously released from LC$^{\rightarrow SDH}$-NA neurons. This would require the use of *Vgat-Cre* or *Hes5-CreERT2* mice, but employing these lines precludes the use of NET-Cre mice, which are necessary for specific and efficient expression of ChrimsonR in LC$^{\rightarrow SDH}$-NA neurons. Nevertheless, all of our experimental data consistently support the proposed model, and we believe that the reviewer will agree with this, without additional experiments that is difficult to conduct because of technical limitations (lines 382-388).

> *(l) As for other experiments, the proportion of Hes+ astrocytes that express hM3Dq, and the absence of expression in other cells, should be quantified and validated to interpret behavioral data.*

We thank the reviewer for raising this point. In our experiments, we used an HA-tag (fused with hM3Dq) to confirm hM3Dq expression. However, it is difficult to precisely analyze individual astrocytes because, as shown in Figure 3J, the boundaries of many HA-tag$^+$ astrocytes are indistinguishable. This seems to be due to the membrane localization of HA-tag, the complex morphology of astrocytes, and their tile-like distribution pattern (Baldwin et al., Trends Cell Biol, 2024 (PMID: 38180380)). Nevertheless, our previous study demonstrated that ~90% of astrocytes in the superficial laminae are Hes5$^+$ (Kohro et al., Nat Neurosci, 2020

(PMID: 33020652)), and intra-SDH injection of AAV-hM3Dq labeled the majority of superficial astrocytes (Figure 3J). Thus, AAV-FLEx[hM3Dq] injection into *Hes5-CreERT2* mice allows efficient expression of hM3Dq in $Hes5^+$ astrocytes in the SDH. Importantly, our previous studies using *Hes5-CreERT2* mice have confirmed that hM3Dq is not expressed in other cell types (neurons, oligodendrocytes, or microglia) (Kohro et al., Nat Neurosci, 2020 (PMID: 33020652); Kagiyama et al., Mol Brain, 2025 (PMID: 40289116)). This information regarding the cell-type specificity has now been briefly described in the revised version (lines 218-219).

> *(m) Showing that the effect of CNO is dose-dependent would strengthen the authors' findings.*

Thank you for your comment. We have now demonstrated a dose-dependent effect of CNO on Ca^{2+} responses in SDH astrocytes (please see our response to Major Point (4) from Reviewer #2 (Recommendations for the Authors) (Figure S7; lines 225-228). In addition, we also confirmed that the effect of CNO is not nonspecific, as CNO application did not alter sIPSCs in spinal cord slices prepared from mice lacking hM3Dq expression in astrocytes (Figure S7; lines 225-228).

> *(n) The proportion of SG neurons for which CNO bath application resulted in a reduction in recorded sIPSCs is not clear.*

We have included individual data points in each bar graph to more clearly illustrate the effect of CNO on each neuron (Figure 3L, N).

> *(o) A1Rs. The specific expression of Cas9 and guide RNAs, and the specific KD of A1Rs, in inhibitory interneurons but not in other cell types expressing A1Rs should be quantified and validated.*

In addition to the data demonstrating the specific expression of SaCas9 and sgAdora1 in $Vgat^+$ inhibitory neurons shown in Figure 3G of the initial version, we have now conducted the same experiments with a different sample and confirmed this specificity: SaCas9 (detected via HA-tag) and sgAdora1 (detected via mCherry) were expressed in $PAX2^+$ inhibitory neurons (Author response image 1). Furthermore, as shown in Figure 3H and I in the initial version, the functional reduction of A_1Rs in inhibitory neurons was validated by electrophysiological recordings. Together, these results support the successful deletion of A_1Rs in inhibitory neurons.

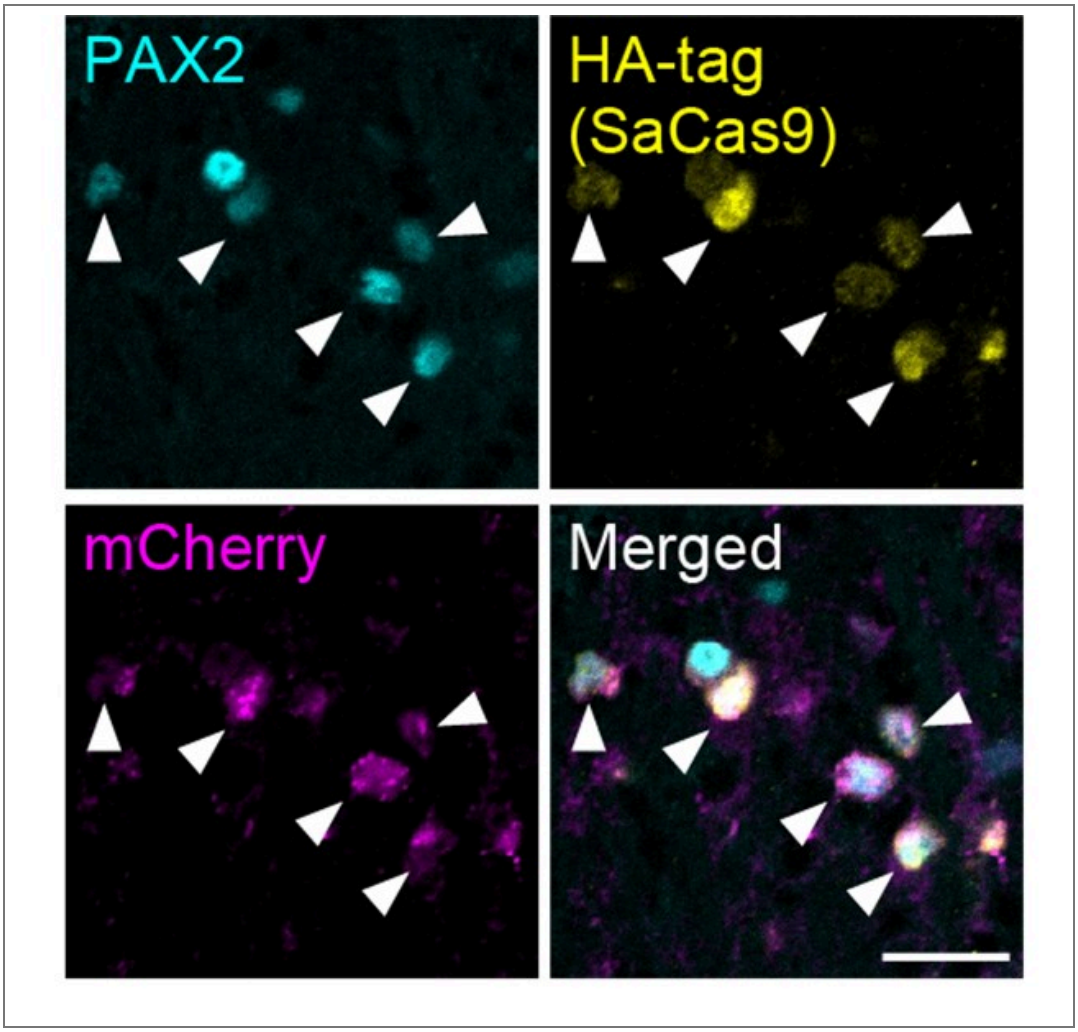

Author response image 1. Expression of HA-tag and mCherry in inhibitory neurons (a different sample from Figure 3G) SaCas9 (yellow, detected by HA-tag) and mCherry (magenta) expression in the PAX2^{+} inhibitory neurons (cyan) at 3 weeks after intra-SDH injection of AAV-FLEx[SaCas9-HA] and AAV-FLEx[mCherry]-U6-sgAdora1 in *Vgat-Cre* mice. Arrowheads indicate genome-editing Vgat^{+} cells. Scale bar, 25 μm.

> *(6) Methods:*
>
> *It is unclear how fiber photometry is performed using "optic cannula" during restraint stress while mice are in a 50ml falcon tube (as shown in Figure 1A).*

We apologize for the omission of this detail in the Methods section. To monitor Ca^{2+} events in LC-NA neurons during restraint stress, we created a narrow slit on the top of the conical tube, allowing mice to undergo restraint stress while connected to the optic fiber (see video). This information has now been added to the Methods section (lines 552-553).

> ***Recommendations for the authors:***
>
> ***Reviewer #1 (Recommendations for the authors):***
>
> *(1) Scientific rigor:*
>
> *It is unclear if the normal distribution of the data was determined before selecting statistical tests.*

We apologize for omitting this description. For all statistical analyses in this study, we first assessed the normality of the data and then selected appropriate statistical tests accordingly. We have added this information to the revised manuscript (lines 711-712).

> *(2) Nomenclature:*
>
> *(a) Mouse Genome Informatics (MGI) nomenclature should be used to describe mouse genotypes (i.e., gene name in italic, only first letter is capitalized, alleles in superscript).*
>
> *(b) FLEx should be used instead of flex.*

Thank you for the suggestion. We have corrected these terms (including FLEx) according to MGI nomenclature.

> ***Reviewer #2 (Public review):***
>
> *Summary:*
>
> *This study investigates the role of spinal astrocytes in mediating stress-induced pain hypersensitivity, focusing on the LC (locus coeruleus)-to-SDH (spinal dorsal horn) circuit and its mechanisms. The authors aimed to delineate how LC activity contributes to spinal astrocytic activation under stress conditions, explore the role of noradrenaline (NA) signaling in this process, and identify the downstream astrocytic mechanisms that influence pain hypersensitivity.*
>
> *The authors provide strong evidence that 1-hour restraint stress-induced pain hypersensitivity involves the LC-to-SDH circuit, where NA triggers astrocytic calcium activity via alpha1a adrenoceptors (alpha1aRs). Blockade of alpha1aRs on astrocytes - but not on Vgat-positive SDH neurons - reduced stress-induced pain hypersensitivity. These findings are rigorously supported by well-established behavioral models and advanced genetic techniques, uncovering the critical role of spinal astrocytes in modulating stress-induced pain.*
>
> *However, the study's third aim - to establish a pathway from astrocyte alpha1aRs to adenosine-mediated inhibition of SDH-Vgat neurons - is less compelling. While pharmacological and behavioral evidence is intriguing, the ex vivo findings are indirect and lack a clear connection to the stress-induced pain model. Despite these limitations, the study advances our understanding of astrocyte-neuron interactions in stress-pain contexts and provides a strong foundation for future research into glial mechanisms in pain hypersensitivity.*
>
> *Strengths:*
>
> *The study is built on a robust experimental design using a validated 1-hour restraint stress model, providing a reliable framework to investigate stress-induced pain hypersensitivity. The authors utilized advanced genetic tools, including retrograde AAVs, optogenetics, chemogenetics, and subpopulation-specific knockouts, allowing precise manipulation and interrogation of the LC-SDH circuit and astrocytic roles in pain modulation. Clear evidence demonstrates that NA triggers astrocytic calcium activity via alpha1aRs, and blocking these receptors effectively reduces stress-induced pain hypersensitivity.*
>
> *Weaknesses:*
>
> *Despite its strengths, the study presents indirect evidence for the proposed NA-to-astrocyte(alpha1aRs)-to-adenosine-to-SDH-Vgat neurons pathway, as the link between astrocytic adenosine release and stress-induced pain remains unclear. The ex vivo*

> *experiments, including NA-induced depolarization of Vgat neurons and chemogenetic stimulation of astrocytes, are challenging to interpret in the stress context, with the high CNO concentration raising concerns about specificity. Additionally, the role of astrocyte-derived D-serine is tangential and lacks clarity regarding its effects on SDH Vgat neurons. The astrocyte calcium signal "dip" after LC optostimulation-induced elevation are presented without any interpretation.*

We appreciate the reviewer's careful reading of our paper. According to the reviewer's comments, we have performed new additional experiments and added some discussion in the revised manuscript (please see the point-by-point responses below).

> ***Reviewer #2 (Recommendations for the authors):***
>
> *The astrocyte-mediated pathway of NA-to-astrocyte (alpha1aRs)-to-adenosine-to-SDH Vgat neurons (A1R) in the context of stress-induced pain hypersensitivity requires more direct evidence. While the data showing that the A1R agonist CPT inhibits stress-induced hypersensitivity and that stress combined with Aβ fiber stimulation increases pERK in the SDH are intriguing, these findings primarily support the involvement of A1R on Vgat neurons and are only behaviorally consistent with SDH-Vgat neuronal A1R knockdown. The role of astrocytes in this pathway in vivo remains indirect. The ex vivo chemogenetic Gq-DREADD stimulation of SDH astrocytes, which reduced sIPSCs in Vgat neurons in a CPT-dependent manner, needs revision with non-DREADD+CNO controls to validate specificity. Furthermore, the ex vivo bath application of NA causing depolarization in Vgat neurons, blocked by CPT, adds complexity to the data leaving me wondering how astrocytes are involved in such processes, and it does not directly connect to stress-induced pain hypersensitivity. These findings are potentially useful but require additional refinement to establish their relevance to the stress model.*

We thank the reviewer for the insightful feedback. First, regarding the role of astrocytes in this pathway in vivo, we showed in the initial version that mechanical pain hypersensitivities induced by intrathecal NA injection and by acute restraint stress were attenuated by both pharmacological blockade and Vgat$^+$ neuron-specific knockdown of A_1Rs (Figure 4A, B). Given that NA- and stress-induced pain hypersensitivity is mediated by α_{1A}R-dependent signaling in Hes5$^+$ astrocytes (Kohro et al., Nat Neurosci, 2020 (PMID: 33020652); this study), these findings provide in vivo evidence supporting the involvement of the NA → Hes5$^+$ astrocyte (via α_{1A}Rs) → adenosine → Vgat$^+$ neuron (via A_1Rs) pathway. As noted in the reviewer's major comment (2), in vivo monitoring of adenosine dynamics in the SDH during stress exposure would further substantiate the astrocyte-to-neuron signaling pathway. However, we did not detect clear signals, potentially due to several technical limitations (see our response below). Acknowledging this limitation, we have now added a new paragraph in the end of Discussion section to address this issue. Second, the specificity of the effect of CNO has now been validated by additional experiments (see our response to major point (4)). Third, the reviewer's concern regarding the action of NA on Vgat$^+$ neurons has also been addressed (see our response to major point (3) below).

> *Major points:*
>
> *(1) The in vivo pharmacology using DCK to antagonize D-serine signaling from alpha1a-activated astrocytes is tangential, as there is limited evidence on how Vgat neurons (among many others) respond to D-serine. This aspect requires more focused exploration to substantiate its relevance.*

We propose that the site of action of D-serine in our neural circuit model is the NMDA receptors (NMDARs) on excitatory neurons, a notion supported by our previous findings (Kohro et al., Nat Neurosci, 2020 (PMID: 33020652); Kagiyama et al., Mol Brain, 2025 (PMID: 40289116)). However, we cannot exclude the possibility that D-serine also acts on NMDARs

expressed by Vgat^{+} inhibitory neurons. Nevertheless, given that intrathecal injection of D-serine in naïve mice induces mechanical pain hypersensitivity (Kohro et al., Nat Neurosci, 2020 (PMID: 33020652)), it appears that the pronociceptive effect of D-serine in the SDH is primarily associated with enhanced pain processing and transmission, presumably via NMDARs on excitatory neurons. We have added this point to the Discussion section in the revised manuscript (lines 325-330).

> *(2) Additionally, employing GRAB-Ado sensors to monitor adenosine dynamics in SDH astrocytes during NA signaling would significantly strengthen conclusions about astrocyte-derived adenosine's role in the stress model.*

We agree with the reviewer's comment. Following this suggestion, we attempted to visualize NA-induced adenosine (and ATP) dynamics using GRAB-ATP and GRAB-Ado sensors (Wu et al., Neuron, 2022 (PMID: 34942116); Peng et al., Science, 2020 (PMID: 32883833)) in acutely isolated spinal cord slices from mice after intra-SDH injection of AAV-hSyn-GRABATP$_{1.0}$ and -GRABAdo$_{1.0}$. We confirmed expression of these sensors in the SDH (Author response image 2a) and observed increased signals after bath application of ATP (0.1 or 1 μM) or adenosine (1 μM) (Author response image 2b, c). However, we were unable to detect clear signals following NA stimulation (Author response image 2b, c). The reason for this lack of detectable changes remains unclear. If the release of adenosine from astrocytes is a highly localized phenomenon, it may be measurable using high-resolution microscopy capable of detecting adenosine levels at the synaptic level and more sensitive sensors. Further investigation will therefore be required (lines 340-341).

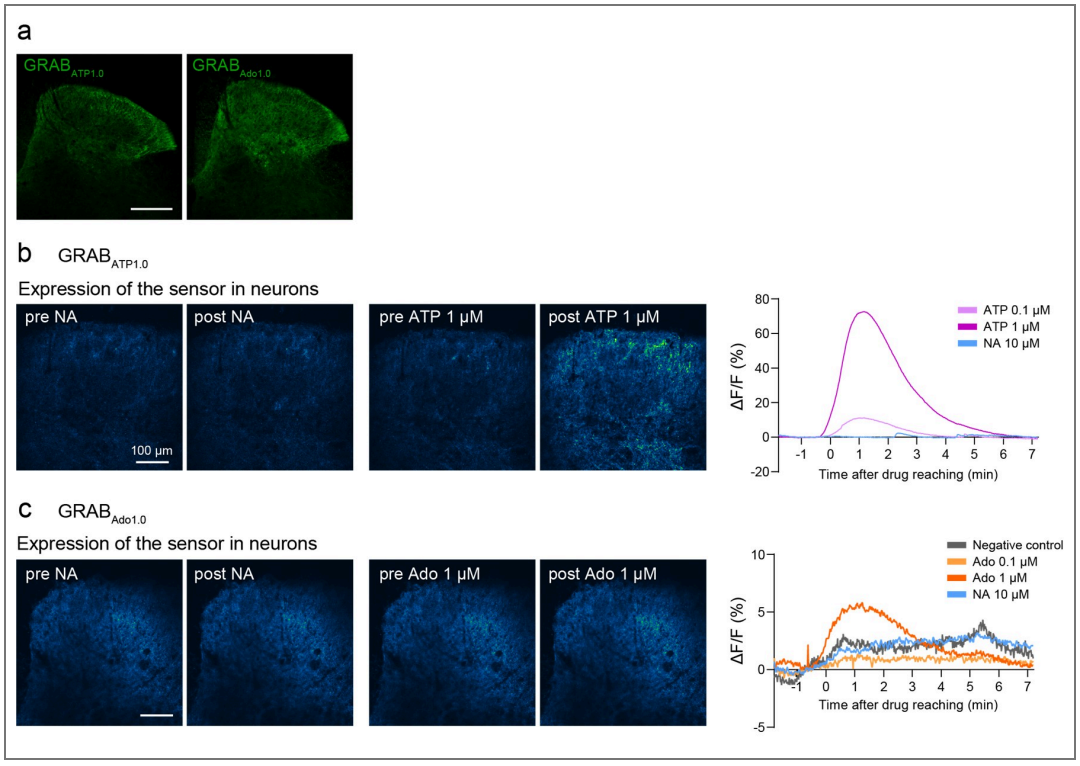

Author response image 2. Ex vivo imaging of GRAB-ATP and GRAB-Ado sensors. (a) Representative images of GRAB$_{ATP1.0}$ (left, green) or GRAB$_{Ado1.0}$ (right, green) expression in the SDH at 3 weeks after SDH injection of AAV-hSyn-GRAB$_{Ado1.0}$ or AAV-hSyn-GRAB$_{Ado1.0}$ in *Hes5-CreERT2* mice. Scale bar, 200 μm. (b) Left: Representative fluorescence images showing GRAB$_{ATP1.0}$ responses before and after perfusion with NA or ATP. Right: Representative traces showing responses to ATP (0.1 and 1 μM) or NA (10 μM). (c) Left: Representative fluorescence images showing GRABAdo1.0 responses before and after perfusion with NA or adenosine (Ado).

Right: Representative traces showing responses to Ado (0.01, 0.1, and 1 μM), NA (10 μM), or no application (negative control).

> *(3) The interpretation of Figure 3D is challenging. The manuscript implies that 20 μM NA acts on Adra1a receptors on Vgat neurons to depolarize them, but this concentration should also activate Adra1a on astrocytes, leading to adenosine release and potential inhibition of depolarization. The observation of depolarization despite these opposing mechanisms requires explanation, as does the inhibition of depolarization by bath-applied A1R agonist. Of note, 20 μM NA is a high concentration for Adra1a activation, typically responsive at nanomolar levels. The discussion should reconcile this with prior studies indicating dose-dependent effects of NA on pain sensitivity (e.g., Reference 22).*

Like the reviewer, we also considered that bath-applied NA could activate α_{1A}Rs expressed on Hes5$^+$ astrocytes. To clarify this point, we have performed additional patch-clamp recordings and found that knockdown of A_1Rs in Vgat$^+$ neurons tended to increase the proportion of Vgat$^+$ neurons with NA-induced depolarizing responses (Figure S8). Therefore, it is conceivable that NA-induced excitation of Vgat$^+$ neurons may involve both a direct effect of NA activating α_{1A}Rs in Vgat$^+$ neurons and an indirect inhibitory signaling from NA-stimulated Hes5$^+$ astrocytes via adenosine (lines 298-300).

The concentration of NA used in our ex vivo experiments is higher than that typically used in vitro with αR-$_{1A}$expressing cell lines or primary culture cells, but is comparable to concentrations used in other studies employing spinal cord slices (Kohro et al., Nat Neurosci, 2020 (PMID: 33020652); Baba et al., Anesthesiology, 2000 (PMID: 10691236); Lefton et al., Science, 2025 (PMID: 40373122)). In slice experiments, drugs must diffuse through the tissue to reach target cells, resulting in a concentration gradient. Therefore, higher drug concentrations are generally necessary in slice experiments, in contrast to cultured cell experiments, where drugs are directly applied to target cells. Importantly, we have previously shown that the pharmacological effects of 20 μM NA on Vgat$^+$ neurons and Hes5$^+$ astrocytes are abolished by loss of α_{1A}Rs in these cells (Uchiyama et al., Mol Brain, 2022 (PMID: 34980215); Kohro et al., Nat Neurosci, 2020 (PMID: 33020652)), confirming the specificity of these NA actions.

Regarding the dose-dependent effect of NA on pain sensitivity, NA-induced pain hypersensitivity is abolished in Hes5$^+$ astrocyte-specific α_{1A}R-KO mice (Kohro et al., Nat Neurosci, 2020 (PMID: 33020652)), indicating that this behavior is mediated by α_{1A}Rs expressed on Hes5$^+$ astrocytes. In contrast, the suppression of pain sensitivity by high doses of NA was unaffected in the KO mice (Kohro et al., Nat Neurosci, 2020 (PMID: 33020652)), suggesting that other adrenergic receptors may contribute to this phenomenon. Clarifying the responsible receptors will require future investigation.

> *(4) In Figure 3K-M, the CNO concentration used (100 μM) is unusually high compared to standard doses (1 to a few μM), raising concerns about potential off-target effects. Including non-hM3Dq controls and using lower CNO concentrations are essential to validate the specificity of the observed effects. Similarly, the study should clarify whether astrocyte hM3Dq stimulation alone (without NA) would induce hyperpolarization in Vgat neurons and how this interacts with NA-induced depolarization.*

We acknowledge that the concentration of CNO used in our experiments is relatively high compared to that used in other reports. However, in our experiments, application of CNO at 1, 10, and 100 μM induced Ca^{2+} increases in GCaMP6-expressing astrocytes in spinal cord slices in a concentration-dependent manner (Figure S7). Among these, 100 μM CNO most effectively replicated the NA-induced Ca^{2+} signals in astrocytes. Based on these findings, we selected this concentration for use in both the current and previous studies (Kohro et al., Nat Neurosci., 2020 (PMID: 33020652)). Importantly, to rule out non-specific effects, we conducted

control experiments using spinal cord slices from mice that did not express hM3Dq in astrocytes and confirmed that CNO had no effect on Ca^{2+} responses in astrocytes and sIPSCs in substantial gelatinosa (SG) neurons (Figure S7; lines 223-228). Thus, although the CNO concentration used is relatively high, the observed effects of CNO are not non-specific but result from the chemogenetic activation of hM3Dq-expressing astrocytes.

In this study, we used *Hes5-CreERT2* and *Vgat-Cre* mice to manipulate gene expression in $Hes5^{+}$ astrocytes and $Vgat^{+}$ neurons, respectively. In order to fully address the reviewer's comment, the use of both Cre lines is necessary. However, simultaneous and independent genetic manipulation in each cell type using Cre activity alone is not feasible with the current genetic tools. We have mentioned this as a technical limitation in the Discussion section (lines 382-388).

> *(5) The role of D-serine released by hM3Dq-stimulated astrocytes in (separately) modulating sub-types of neurons including excitatory neurons and Vgat positives needs more detailed discussion. If no effect of D-serine on Vgat neurons is observed, this should be explicitly stated, and the discussion should address why this might be the case.*

As mentioned in our response to Major Point (1) above, we have added a discussion of this point in the revised manuscript (lines 325-330).

> *(6) Finally, the observed "dip" in astrocyte calcium signals below baseline following the large peaks with LC optostimulation should be discussed further, as understanding this phenomenon could provide valuable insights into astrocytic signaling dynamics in the context of single acute or repetitive chronic stress.*

Thank you for your comment. We found that this phenomenon was not affected by pretreatment with the α_{1A}R-specific antagonist silodosin (Author response image 3), which effectively suppressed Ca^{2+} elevations evoked by stimulation of LC-NA neurons (Figure 2F). This implies that the phenomenon is independent of α_{1A}R signaling. Elucidating the detailed underlying mechanism remains an important direction for future investigation.

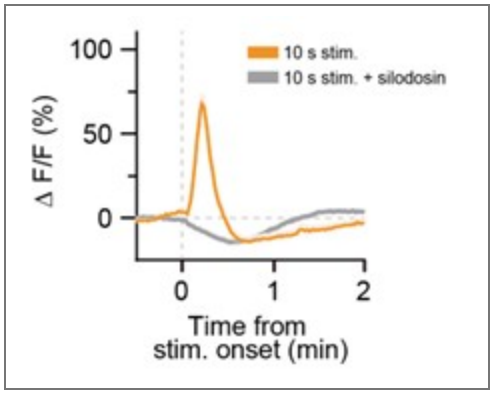

Author response image 3. The observed "dip" in astrocyte Ca^{2+} signals was not affected by pretreatment with the α_{1A}R-specific antagonist silodosin. Representative traces of astrocytic GCaMP6m signals in response to optogenetic stimulation of LC-NAe$^{\rightarrow SDH}$rgic axons/terminals in a spinal cord slice. Each trace shows the GCaMP6m signal before and after optogenetic stimulation (625 nm, 1 mW, 10 Hz, 5 ms pulse duration, 10 s). Slices were pretreated with silodosin (40 nM) for 5 min prior to stimulation.

> ***Reviewer #3 (Public review):***
>
> *Summary:*

This is an exciting and timely study addressing the role of descending noradrenergic systems in nocifensive responses. While it is well-established that spinally released noradrenaline (aka norepinephrine) generally acts as an inhibitory factor in spinal sensory processing, this system is highly complex. Descending projections from the A6 (locus coeruleus, LC) and the A5 regions typically modulate spinal sensory processing and reduce pain behaviours, but certain subpopulations of LC neurons have been shown to mediate pronociceptive effects, such as those projecting to the prefrontal cortex (Hirshberg et al., PMID: 29027903).

The study proposes that descending cerulean noradrenergic neurons potentiate touch sensation via alpha-1 adrenoceptors on Hes5+ spinal astrocytes, contributing to mechanical hyperalgesia. This finding is consistent with prior work from the same group (dd et al., PMID:). However, caution is needed when generalising about LC projections, as the locus coeruleus is functionally diverse, with differences in targets, neurotransmitter co-release, and behavioural effects. Specifying the subpopulations of LC neurons involved would significantly enhance the impact and interpretability of the findings.

Strengths:

The study employs state-of-the-art molecular, genetic, and neurophysiological methods, including precise CRISPR and optogenetic targeting, to investigate the role of Hes5+ astrocytes. This approach is elegant and highlights the often-overlooked contribution of astrocytes in spinal sensory gating. The data convincingly support the role of Hes5+ astrocytes as regulators of touch sensation, coordinated by brain-derived noradrenaline in the spinal dorsal horn, opening new avenues for research into pain and touch modulation.

Furthermore, the data support a model in which superficial dorsal horn (SDH) Hes5+ astrocytes act as non-neuronal gating cells for brain-derived noradrenergic (NA) signalling through their interaction with substantia gelatinosa inhibitory interneurons. Locally released adenosine from NA-stimulated Hes5+ astrocytes, following acute restraint stress, may suppress the function of SDH-Vgat+ inhibitory interneurons, resulting in mechanical pain hypersensitivity. However, the spatially restricted neuron-astrocyte communication underlying this mechanism requires further investigation in future studies.

Weaknesses

(1) Specificity of the LC Pathway targeting

The main concern lies with how definitively the LC pathway was targeted. Were other descending noradrenergic nuclei, such as A5 or A7, also labelled in the experiments? The authors must convincingly demonstrate that the observed effects are mediated exclusively by LC noradrenergic terminals to substantiate their claims (i.e. "we identified a circuit, the descending LC→SDH-NA neurons").

(a) For instance, the direct vector injection into the LC likely results in unspecific effects due to the extreme heterogeneity of this nucleus and retrograde labelling of the A5 and A7 nuclei from the LC (i.e., Li et al., PMID: 26903420).

We appreciate the reviewer's valuable comments. To address this point, we performed additional experiments and demonstrated that intra-SDH injection of AAVretro-Cre followed by intra-LC injection of AAV2/9-EF1α-FLEx[DTR-EGFP] specifically results in DTR expression in NA neurons of the LC, but not of the A5 or A7 regions (Figure S4; lines 127-128). These results confirm the specificity of targeting the LC$^{\rightarrow SDH}$-NAergic pathway in our study.

> *(b) It is difficult to believe that the intersectional approach described in the study successfully targeted LC→SDH-NA neurons using AAVrg vectors. Previous studies (e.g., PMID: 34344259 or PMID: 36625030) demonstrated that similar strategies were ineffective for spinal-LC projections. The authors should provide detailed quantification of the efficiency of retrograde labelling and specificity of transgene expression in LC neurons projecting to the SDH.*

Thank you for your comment. As we described in our response to the weakness (5)-e) of Reviewer #1 (Public review), our additional analysis showed that, under our experimental conditions, expression of genes (for example DTR) was observed in 4.4% of NA (TH^+) neurons in the LC (Figure S4; lines 126-127).

The reasons for this difference between the previous studies and our current study is unclear; however, it is likely attributed to methodological differences, including the type of viral vectors employed, species differences (mouse (PMID: 34344259, our study) vs. rat (PMID: 36625030)), the amount of AAV injected into the SDH (300 nL at three sites (PMID: 34344259), and 300 nL at a single site (our study)) and LC (500 nL at a single site (PMID: 34344259), and 300 nL at a single site (our study)), as well as the depth of AAV injection in the SDH (200–300 μm from the dorsal surface of the spinal cord (PMID: 34344259), and 120–150 μm in depth from the surface of the dorsal root entry zone (our study)).

> *(c) Furthermore, it is striking that the authors observed a comparably strong phenotypical change in Figure 1K despite fewer neurons being labelled, compared to Figure 1H and 1N with substantially more neurons being targeted. Interestingly, the effect in Figure 1K appears more pronounced but shorter-lasting than in the comparable experiment shown in Figure 1H. This discrepancy requires further explanation.*

Although only a representative section of the LC was shown in the initial version, $LC^{\rightarrow SDH}$-NA neurons are distributed rostrocaudally throughout the LC, as previously reported (Llorca-Torralba et al., Brain, 2022 (PMID: 34373893)). Our additional experiments analyzing multiple sections of the anterior and posterior regions of the LC have now revealed that approximately sixty $LC^{\rightarrow SDH}$-NA neurons express DTR, and these neurons are eliminated following DTX treatment (Figure S4; lines 126-128) (it should be noted that these neurons specifically project to the L4 segment of the SDH, and the total number of $LC^{\rightarrow SDH}$-NA neurons is likely much higher). Considering the specificity of $LC^{\rightarrow SDH}$-NAergic pathway targeting demonstrated in our study (as described above), together with the fact that primary afferent sensory fibers from the plantar skin of the hindpaw predominantly project to the L4 segment of the SDH, these data suggest that the observed behavioral changes are attributable to the loss of these neurons and that ablation of even a relatively small number of NA neurons in the LC can have a significant impact on behavior. We have added this hypothesis in the Discussion section (lines 373-382).

Regarding the data in Figures 1H and 1K, as the reviewer pointed out, a statistically significant difference was observed at 90 min in mice with ablation of LC-NA neurons, but not in those with $LC^{\rightarrow SDH}$-NA neuron ablation. This is likely due to a slightly higher threshold in the control group at this time point (Figure 1K), and it remains unclear whether there is a mechanistic difference between the two groups at this specific time point.

> *(d) A valuable addition would be staining for noradrenergic terminals in the spinal cord for the intersectional approach (Figure 1J), as done in Figures 1F/G. LC projections terminate preferentially in the SDH, whereas A5 projections terminate in the deep dorsal horn (DDH). Staining could clarify whether circuits beyond the LC are being ablated.*

As suggested, we performed DTR immunostaining in the SDH; however, we did not detect any DTR immunofluorescence there. A similar result was also observed in the spinal terminals of DTR-expressing primary afferent fibers (our unpublished data). The reason for this is

unclear, but to the best of our knowledge, no studies have clearly shown DTR expression at presynaptic terminals, which may be because the action of DTX on the neuronal cell body is necessary for cell ablation. Nevertheless, as described in our response to the weakness (5)-f) by Reviewer 1 (Public review), we have now confirmed the specific expression of DTR in the LC, but not in the A5 and A7 regions (Figure S4; lines 127-128).

> *(e) Furthermore, different LC neurons often mediate opposite physiological outcomes depending on their projection targets-for example, dorsal LC neurons projecting to the prefrontal cortex PFCx are pronociceptive, while ventral LC neurons projecting to the SC are antinociceptive (PMIDs: 29027903, 34344259, 36625030). Given this functional diversity, direct injection into the LC is likely to result in nonspecific effects.*

To avoid behavioral outcomes resulting from a mixture of facilitatory and inhibitory effects caused by activating the entire population of LC-NA neurons, we employed a specific manipulation targeting LC$^{\rightarrow SDH}$-NA neurons using AAV vectors. The specificity of this manipulation was confirmed in our previous study (Kohro et al., Nat Neurosci, 2020 (PMID: 33020652)) and in the current study (Figure S4). Using this approach, we previously demonstrated that LC neurons can exert pronociceptive effects via astrocytes in the SDH (Kohro et al., Nat Neurosci, 2020 (PMID: 33020652)). This pronociceptive role is further supported by the current study, which uses a more selective manipulation of LC$^{\rightarrow SDH}$-NA neurons through a *NET-Cre* mouse line. In addition, intrathecal administration of relatively low doses of NA in naïve mice clearly induces mechanical pain hypersensitivity. Nevertheless, we have also acknowledged that several recent studies have reported an inhibitory role of LC$^{\rightarrow SDH}$-NA neurons in spinal nociceptive signaling. The reason for these differing behavioral outcomes remains unclear, but several methodological differences may underlie the discrepancy. First, the degree of LC$^{\rightarrow SDH}$-NA neuronal activity may play a role. Although direct comparisons between studies reporting pro- and anti-nociceptive effects are difficult, our previous studies demonstrated that intrathecal administration of high doses of NA in naïve mice does not induce mechanical pain hypersensitivity (Kohro et al., Nat Neurosci, 2020 (PMID: 33020652)). Second, the sensory modality used in behavioral testing may be a contributing factor as the pronociceptive effect of NA appears to be selectively observed in responses to mechanical, but not thermal, stimuli (Kohro et al., Nat Neurosci, 2020 (PMID: 33020652)). This sensory modality-selective effect is also evident in mice subjected to acute restraint stress (Table S1). Therefore, the role of LC$^{\rightarrow SDH}$-NA neurons in modulating nociceptive signaling in the SDH is more complex than previously appreciated, and their contribution to pain regulation should be reconsidered in light of factors such as NA levels, sensory modality, and experimental context. In revising the manuscript, we have included some points described above in the Discussion (lines 282-291).

> *Conclusion on Specificity: The authors are strongly encouraged to address these limitations directly, as they significantly affect the validity of the conclusions regarding the LC pathway. Providing more robust evidence, acknowledging experimental limitations, and incorporating complementary analyses would greatly strengthen the manuscript.*

We appreciate the reviewer's comments. We fully acknowledge the limitations raised and agree that addressing them directly is important for the rigor of our conclusions on the LC pathway. To this end, we have performed additional experiments (e.g., Figure A and S4), which are now included in the revised manuscript. Furthermore, we have also newly added a new paragraph for experimental limitations in the end of Discussion section (lines 373-408). We believe these new data substantially strengthen the validity of our findings and have clarified these points in the Discussion section.

> *(2) Discrepancies in Data*

> *(a) Figures 1B and 1E: The behavioural effect of stress on PWT (Figure 1E) persists for 120 minutes, whereas Ca2+ imaging changes (Figure 1B) are only observed in the first 20 minutes, with signal attenuation starting at 30 minutes. This discrepancy requires clarification, as it impacts the proposed mechanism.*

Thank you for your important comment. As pointed out by the reviewer, there is a difference between the duration of behavioral responses and Ca^{2+} events, although the exact time point at which the PWT begins to decline remains undetermined (as behavioral testing cannot be conducted during stress exposure). A similar temporal difference was also observed following intraplantar injection of capsaicin (Kohro et al., Nat Neurosci, 2020 (PMID: 33020652)); while $LC^{\rightarrow SDH}$-NA neuron-mediated astrocytic Ca^{2+} responses in SDH astrocytes last for 5–10 min after injection, behavioral hypersensitivity peaks around 60 min post-injection and gradually returns to baseline over the subsequent 60–120 min. These findings raise the possibility that astrocyte-mediated pain hypersensitivity in the SDH may involve a sustained alteration in spinal neural function, such as central sensitization. We have added this hypothesis to the Discussion section of the revised manuscript (lines 399-408), as it represents an important direction for future investigation.

> *(b) Figure 4E: The effect is barely visible, and the tissue resembles "Swiss cheese," suggesting poor staining quality. This is insufficient for such an important conclusion. Improved staining and/or complementary staining (e.g., cFOS) are needed. Additionally, no clear difference is observed between Stress+Ab stim. and Stress+Ab stim.+CPT, raising doubts about the robustness of the data.*

As suggested, we performed c-FOS immunostaining and obtained clearer results (Figure 4E,F; lines 243-252). We also quantitatively analyzed the number of $c\text{-}FOS^{+}$ cells in the superficial laminae, and the results are consistent with those obtained from the pERK experiments.

> *(c) Discrepancy with Existing Evidence: The claim regarding the pronociceptive effect of LC→SDH-NAergic signalling on mechanical hypersensitivity contrasts with findings by Kucharczyk et al. (PMID: 35245374), who reported no facilitation of spinal convergent (wide-dynamic range) neuron responses to tactile mechanical stimuli, but potent inhibition to noxious mechanical von Frey stimulation. This discrepancy suggests alternative mechanisms may be at play and raises the question of why noxious stimuli were not tested.*

In our experiments, ChrimsonR expression was observed in the superficial and deeper laminae of the spinal cord (Figure S6). Due to the technical limitations of the optical fibers used for optogenetics, the light stimulation could only reach the superficial laminae; therefore, it may not have affected the activity of neurons (including WDR neurons) located in the deeper laminae. Furthermore, the study by Kucharczyk et al. (Brain, 2022 (PMID: 35245374)) employed a stimulation protocol that differed from ours, applying continuous stimulation over several minutes. Given that the levels of NA released from $LC^{\rightarrow SDH}$-NAergic terminals in the SDH increase with the duration of terminal stimulation (as shown in Figure 2B), longer stimulation may result in higher levels of NA in the SDH. Considering also our data indicating that the pro- and anti-nociceptive effects of NA are dose dependent (Kohro et al., Nat Neurosci, 2020 (PMID: 33020652)), these differences may be related to $LC^{\rightarrow SDH}$-NA neuron activity, NA levels in the SDH, and the differential responses of SDH neurons in the superficial versus deeper laminae (lines 388-395).

> *(3) Sole reliance on Von Frey testing*
>
> *The exclusive use of von Frey as a behavioural readout for mechanical sensitisation is a significant limitation. This assay is highly variable, and without additional supporting measures, the conclusions lack robustness. Incorporating other behavioural measures, such as the adhesive tape removal test to evaluate tactile discomfort, the needle floor*

> *walk corridor to assess sensitivity to uneven or noxious surfaces, or the kinetic weight-bearing test to measure changes in limb loading during movement, could provide complementary insights. Physiological tests, such as the Randall-Selitto test for noxious pressure thresholds or CatWalk gait analysis to evaluate changes in weight distribution and gait dynamics, would further strengthen the findings and allow for a more comprehensive assessment of mechanical sensitisation.*

Thank you for your suggestion. Based on our previous findings that $Hes5^{+}$ astrocytes in the SDH selectively modulate mechanosensory signaling (Kohro et al., Nat Neurosci, 2020 (PMID: 33020652)), the present study focused on behavioral responses to mechanical stimuli using von Frey filaments. As we have not previously conducted most of the behavioral tests suggested by the reviewers, and as we currently lack the necessary equipments for these tests (e.g., Randall–Selitto test, CatWalk gait analysis, and weight-bearing test), we were unable to include them in this study. However, it will be of great interest in future research to investigate whether activation of the $LC^{\rightarrow SDH}$-NA neuron-to-SDH $Hes5^{+}$ astrocyte signaling pathway similarly sensitizes behavioral responses to other types of mechanical stimuli and also to investigate the sensory modality-selective pro- and antinociceptive role of $LC^{\rightarrow SDH}$-NAergic signaling in the SDH (lines 396-399).

> *Overall Conclusion*
>
> *This study addresses an important and complex topic with innovative methods and compelling data. However, the conclusions rely on several assumptions that require more robust evidence. Specificity of the LC pathway, experimental discrepancies, and methodological limitations (e.g., sole reliance on von Frey) must be addressed to substantiate the claims. With these issues resolved, this work could significantly advance our understanding of astrocytic and noradrenergic contributions to pain modulation.*

We have made every effort to address the reviewer's concerns through additional experiments and analyses. Based on the new control data presented, we believe that our explanation is reasonable and acceptable. Although additional data cannot be provided on some points due to methodological constraints and limitations of the techniques currently available in our laboratory, we respectfully submit that the evidence presented sufficiently supports our conclusions.

> ***Reviewer #3 (Recommendations for the authors):***
>
> *A lot of beautiful and challenging-to-collect data is presented. Sincere congratulations to all the authors on this achievement!*
>
> *Notwithstanding, please carefully reconsider the conclusions regarding the LC pathway, as additional evidence is required to ensure their specificity and robustness.*

We thank the reviewer for the kind comments and for raising an important point regarding the LC pathway. The reviewer's feedback prompted us to conduct additional investigations to further strengthen the validity of our conclusions. We have incorporated these new data and analyses into the revised manuscript, and we believe that these revisions substantially enhance the robustness and reliability of our findings.

https://doi.org/10.7554/eLife.104453.2.sa0